1994ApJ...428..292L

THE ASTROPHYSICAL JOURNAL, 428:292–318, 1994 June 10
© 1994. The American Astronomical Society. All rights reserved. Printed in U.S.A.

GEOMETRY AND PHYSICAL CONDITIONS IN THE STELLAR WIND OF AG CARINAE[1]

CLAUS LEITHERER,[2] RICHARD ALLEN,[3] BRUCE ALTNER,[4] AUGUSTO DAMINELI,[5] LAURENT DRISSEN,[2]
THAIS IDIART,[5] OLIVIA LUPIE,[2] ANTONELLA NOTA,[2,6] CARMELLE ROBERT,[2]
WERNER SCHMUTZ,[7] AND STEVEN N. SHORE[8]
Received 1993 October 6; accepted 1993 December 10

ABSTRACT

AG Carinae is one of the prototypes of the class of Luminous Blue Variables. Since 1990 the star has continuously brightened in its visual continuum. We report on a multi-instrument and -wavelength observing campaign to monitor the current activity phase of AG Car. Ground-based photometry, polarimetry, spectroscopy, and space-ultraviolet spectroscopy and spectropolarimetry have been obtained.

From the variability of the polarization at ultraviolet and optical wavelengths we detect significant intrinsic polarization. $P_{\rm int} \geq 0.5\%$ is a large value for a hot, luminous star, suggesting departures from spherical symmetry in the wind of AG Car. The intrinsic polarization is variable on a timescale of 2 months or less. The measured ultraviolet polarization (intrinsic + interstellar) dropped to 0.5% in 1992 May and returned to 1% in 1992 July. The results are interpreted in terms of a variable outflow with a density enhancement in the equatorial plane. A similar model was suggested for the related object R127 in the Large Magellanic Cloud. This geometry is reminiscent of the large-scale morphology of the gas nebula and dust "jet" surrounding AG Car. It is therefore likely that physical conditions close to the stellar surface are responsible for the geometry of the spatially resolved circumstellar material around AG Car.

The line spectrum in the optical and ultraviolet is dominated by the effects of a massive stellar wind. Two wind components are detected: a slow dense wind, where the bulk of recombination radiation is emitted, and a faster, less dense wind, visible in the absorption components of ultraviolet P Cygni profiles. This wind structure is consistent with the geometry suggested by the spectropolarimetric observations, and it is reminiscent of the wind conditions prevailing in B[e] stars.

An analysis of the photospheric and wind parameters has been performed using an expanding, spherically extended non-LTE model atmosphere. The temperature of AG Car decreased from 21,000 to 14,000 K over $\sim$1 yr, with a corresponding increase of the photospheric radius by a factor of 2. Helium is found to be significantly overabundant, supporting the very evolved state of AG Car. Comparison with evolutionary models leads to an estimate for the zero-age main-sequence mass of $(50 \pm 10)\ M_{\odot}$. Therefore the possibility cannot entirely be excluded that AG Car is in a post–red supergiant phase.

Despite the drastic change of the photospheric conditions, the mass-loss rate did not increase. We find no evidence for a positive correlation between wind density and stellar radius. This makes models that explain the radius increase by opacity effects in the outflow unlikely. The mechanism responsible for the temperature and radius variations is still unknown but most likely has its origin in subphotospheric regions.

Subject headings: polarization — stars: evolution — stars: individual (AG Carinae) — stars: mass loss — supergiants — ultraviolet: stars

1. INTRODUCTION

AG Carinae (=HD 94910 = CoD −59°3430 = CPD −59°2860) is one of the prototypes of the Luminous Blue Variables (LBVs). The class of LBVs has originally been defined by Conti (1984). For a general discussion of the LBV phenomenon, we refer the reader to the proceedings of IAU Colloquium 113 (Davidson, Moffat, & Lamers 1989). In short, LBVs are early-type, luminous stars displaying dramatic photometric and spectroscopic variations over several distinct timescales, ranging between weeks and decades. LBVs as a class of stars are believed to represent a short-lived (10^4–10^5 yr) phase during the evolution of a massive star when a significant amount of mass is lost (Maeder 1989). It is largely the LBV phase which determines the evolutionary relation between O stars on the hydrogen-burning main-sequence and core-helium-burning Wolf-Rayet stars in the theoretical Hertzsprung-Russell diagram. Therefore understanding the physical processes operating during the LBV phase is crucial for modeling the evolution of massive stars in general.

[1] Based on observations with the NASA/ESA *Hubble Space Telescope*, obtained at the Space Telescope Science Institute, which is operated by AURA for NASA under contract NAS 5-26555; on observations with the *International Ultraviolet Explorer* satellite, which is sponsored and operated by the United States National Aeronautics and Space Administration, by the Science Research Council of the United Kingdom, and by the European Space Agency; on observations obtained at the National Laboratory of Astrophysics (LNA/CNP$_q$); and on observations obtained at the European Southern Observatory, La Silla.

[2] Space Telescope Science Institute, 3700 San Martin Drive, Baltimore, MD 21218; leitherer@stsci.edu, drissen@stsci.edu, lupie@stsci.edu, nota@stsci.edu, crobert@stsci.edu

[3] Steward Observatory, University of Arizona, Tucson, AZ 85721; rallen@as.arizona.edu

[4] Applied Research Corporation, 8201 Corporation Drive, Suite 1120, Landover, MD 20758; altner@fosvax.arclch.com

[5] Instituto Astronômico e Geofísico da USP, Caixa Postal 9638, 01065 São Paulo, Brazil; iagusp::damineli, iagusp::thais

[6] Affiliated with the Astrophysics Division, Space Science Department of the European Space Agency.

[7] Institut für Astronomie, ETH-Zentrum, CH-8092 Zürich, Switzerland; schmutz@astro.phys.ethz.ch

[8] Goddard Space Flight Center, Greenbelt, MD 20771; sshore@vines.iusb.indiana.edu

© American Astronomical Society • Provided by the NASA Astrophysics Data System

1994ApJ...428..292L

AG Carinae is the cornerstone for the interpretation of the LBV phenomenon. It has a rich history of observations at various wavelengths (see Nota et al. 1992 for the available literature). Viotti et al. (1984) demonstrated that an increase in brightness at optical wavelengths is accompanied by a corresponding decrease in the ultraviolet. Lamers et al. (1989) studied the visual energy distribution at nine epochs and found that the bolometric magnitude of AG Car remains constant. Observations of other LBVs (e.g., R127: Stahl et al. 1983; S Doradus: Leitherer et al. 1985) are consistent with this result. The constancy of the bolometric luminosity during the variability cycle of LBVs led to the suggestion that drastic changes of the physical conditions in the outer stellar atmospheres result in modified opacities and subsequently a redistribution of the stellar radiation field from shorter to longer wavelengths (Leitherer et al. 1989b). In such a scenario, the mass-loss properties of LBVs would be largely determined by the properties of the underlying star, and radiation pressure could be invoked to account for the observed stellar-wind characteristics (Pauldrach & Puls 1990). This situation would be rather similar to massive main-sequence stars where the theory of radiatively driven winds can predict stellar-wind properties from stellar parameters to a high degree of precision (Kudritzki et al. 1992).

Due to its relative proximity ($D \approx 6$ kpc; Humphreys et al. 1989) AG Car and its environment can be studied in much more detail than possible for the majority of LBVs, which are extragalactic. AG Car is surrounded by an extended nebula first described by Thackeray (1950). Spectroscopic studies by Johnson (1976) and Thackeray (1977) led to the suggestion that the circumstellar material had been ejected by AG Car in an outburst $\sim 10^4$ yr ago. High-resolution coronographic imaging of the inner part of the nebulosities (Paresce & Nota 1989) revealed a bipolar, helical structure originating from—or close to—AG Car itself. This discovery spurred detailed imaging and spatially resolved spectroscopy of other LBVs as well. As a result, ejecta which in several cases show evidence for asymmetries have been detected in the LBVs HR Car (Hutsemékers & Van Drom 1991a), WRA 751 (Hutsemékers & Van Drom 1991b), η Car (Hester et al. 1991), P Cyg (Johnson et al. 1992), and R127 (Clampin et al. 1993).

The discovery of highly asymmetric, bipolar ejecta around AG Car bears important consequences for the interpretation of the mass-loss mechanism in LBVs. If asymmetries in the outflows occur in close vicinity of the star (i.e. within a few stellar radii), geometries breaking spherical symmetry of the system may have to be invoked. Gallagher (1989) discussed models for LBVs which include binaries and/or disklike configurations. Such models face difficulties in accounting quantitatively for several LBV parameters, such as the lifetime of the LBV phase. However, the detection of bipolar outflows in some LBVs has revived the interest in such models. Alternatively, the formation of the bipolar outflow could occur far away from the star due to a nozzle mechanism of the interstellar medium (Raga & Cantó 1989). In the latter case, the observed jetlike structures would not necessarily be indicative of large-scale symmetry breaking close to the stellar surface, and stellar-wind models for single, spherical stars could still be applicable.

Ultraviolet spectropolarimetry, optical polarimetry, ultraviolet spectroscopy, and ground-based spectroscopy of AG Car have been obtained in order to probe the geometry and the physical conditions of the outflow within several stellar radii. The goal of this study is twofold. First, the significance of variabilities and asymmetries in the outflow will be assessed. Second, the correlation between mass loss and photospheric parameters will be addressed. An initial study performed by some of us (Leitherer, Damineli, & Schmutz 1992) indicated that the mass loss from AG Car occurs at a rate which is largely independent of photospheric parameters. This result, if confirmed on the basis of a larger data set, differs drastically from the standard scenario thought to apply to all LBVs. The observations are described in § 2. The polarimetric properties are interpreted in § 3. Section 4 contains a discussion of the photometric and spectroscopic evolution of AG Car during our observing campaign. The stellar and wind parameters are derived from a non-LTE analysis of the spectrum in § 5. In § 6 we discuss the astrophysical significance of the wind properties and its geometry. The conclusions are presented in § 7.

2. OBSERVATIONAL DATA

We are monitoring the current activity cycle of AG Car using photometric, polarimetric, and spectroscopic techniques over a wide spectral range. The visual brightness of AG Car had reached a maximum of $m_V \approx 6.0$ around 1981 when Wolf & Stahl (1982) studied the expanding envelope of the object. Subsequently the visual brightness declined to ~ 8.0 around 1985 as described by Stahl (1986). The spectral type changed from A to late O during this time interval. AG Car remained around $m_V \approx 8.0$ until 1990. In 1991 Kilmartin & Bateson (1991) reported an increase in m_V which is still continuing at present. Figure 1 shows the photometric evolution of AG Car for 1980–1993. The data have been compiled from visual measurements of the Variable Star Section of the Royal Astronomical Society of New Zealand (Bateson 1980–1993). The most recent data points are based on photoelectric measurements in the Johnson BV system obtained at the 50 cm telescope of UFRGS Observatory. The data are listed in Table 1. Typical errors are 0.03 in V and 0.02 in $B-V$. Although the measurements obtained at UFRGS Observatory refer to different photometric system than the New Zealand data (photoelectric vs. visual), the two data sets agree rather well. We estimate that the *average* errors of the visual and photoelectric measurements are ~ 0.1 and 0.03 mag, respectively. The individual errors of the visual data, however, can sometimes be much larger. Each New Zealand data point in Figure 1 is the mean of

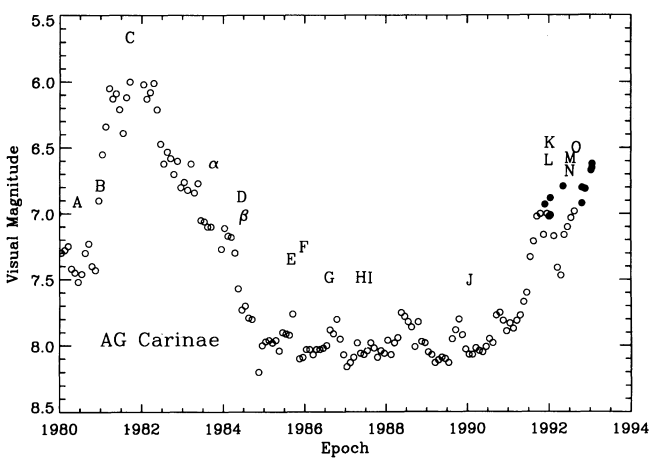

FIG. 1.—Visual light curve of AG Car from 1980 until 1994. Each open circle is the mean of several individual visual estimates. The filled dots denote photoelectric measurements. Letters refer to the *IUE* spectra listed in Table 4.

© American Astronomical Society • Provided by the NASA Astrophysics Data System

1994ApJ...428..292L

TABLE 1

PHOTOMETRY OBTAINED AT UFRGS OBSERVATORY

Epoch	V	$B-V$
1991 Dec 2	6.93	0.66
1992 Jan 3	7.02	0.69
1992 Jan 13	6.88	0.66
1992 May 4	6.79	0.66
1992 Oct 21	6.92	0.68
1992 Oct 22	6.80	0.68
1992 Nov 19	6.81	0.71
1993 Jan 12	6.67	0.67
1993 Jan 20	6.65	0.67
1993 Jan 21	6.62	0.67

the visual measurements by several observers. The number of observers contributing to these measurements varies strongly. Especially during the second half of each year, when AG Car is close to the Sun, the mean value is based on very few observers (less than 5), and systematic effects may become important.

Our spectropolarimetric and spectroscopic observations commenced in late 1990, when AG Car showed the first indication of a rise from its minimum of the light curve.

2.1. *Ultraviolet Spectropolarimetry with HST*

The first UV polarization measurements of AG Car were obtained on three separate visits using the *Hubble Space Telescope* (*HST*) Faint Object Spectrograph (FOS) in its spectropolarimetric mode. The observation details are summarized in Table 2. We used the G270H grating (2200–3400 Å) and "B" waveplate, the combination being most sensitive to linear polarization at ultraviolet wavelengths. A detailed description of the instrumentation may be found in the Faint Object Spectrograph Instrument Handbook (Kinney 1992) and in Allen & Angel (1982).

On each of our three visits to AG Car, we acquired four unique polarization sets (each set consisting of eight waveplate positions) over four orbits, in order to assess instrument stability and data repeatability. During the 1991 November data set (where the 0.″5 aperture was used) spacecraft jitter was appreciable during orbital day/night transitions (confirmed in the pointing telemetry). We eliminated those specific waveplate positions where jitter significantly reduced the flux. All other common waveplate spectra over the four orbits agreed to within photon statistics. (This implies that at least over a few hours, the polarization appears to remain constant).

Because each orthogonal sense of polarization is not measured simultaneously by the FOS and each falls on a different place on the photocathode, each beam must be reduced independently using the flat field, wavelength and sensitivity calibrations (obtained through the polarizers) supplied in the STScI Calibration Data Base. The polarization processing was done using the code developed by Allen and described in the FOS Science Verification Report. The processing was performed on each beam separately and combined later. The retardation of the waveplates, pass direction of the Wollastons, and offset of the waveplates were calibrated on the ground and verified in-flight (Allen & Smith 1992). Errors in the retardation calibration produce systematic errors in the measured polarization. For grating H27, these errors should be less than 0.02 times the measured linear polarization. A 1% linear polarization could thus be uncertain by $\pm 0.02\%$. A minor oscillation in θ also occurs because of a slight misalignment of the two halves of the waveplate. While some of this oscillation is taken out in the data processing, residual errors of $\pm 1°$ are possible. Allen et al. (1993) found the instrumental polarization to be less than 0.1% overall. Our reported polarization and position angle error estimates are based only on the photon statistics of the observations.

Immediately following each visit to AG Car, we obtained a single short polarization data set on the B1V polarization standard BD +64°106 (Lupie & Stockman 1988; Schmidt, Elston, & Lupie 1992) using the same polarization mode but with the 4.″3 aperture (to increase signal and minimize precious *HST* exposure time). Table 3 lists the error-weighted mean polarization, average errors, rms deviation, polarization (inverse) signal-to-noise parameter ϵ_P/P, error-weighted mean position angle, errors, and rms deviation. The data on the three occasions agree to within observational error. The polarization and position angle in the UV (bins of 300 Å to improve S/N) and optical (from Schmidt, Elston, & Lupie 1992) are presented as a function of wavelength in Figure 2.

The solid line is a fit to the optical data and extrapolated to the UV. The fit is based on the Wilking modification to Serkowski's law (Serkowski, Mathewson, & Ford 1975 [hereafter SMF]; Wilking, Lebofsky, & Rieke 1982). The Serkowski relation describes the wavelength dependence of the polarization as a function of P_{max} and λ_{max}.

Data obtained with the Wisconsin Ultraviolet Photo-Polarimeter experiment (WUPPE; Clayton et al. 1992) toward several sight lines revealed that although the polarization decreases, there is "substantial variation" in the wavelength dependence in the UV. Some stars followed the Serkowski extrapolation while others showed excess polarization at the shorter wavelengths. Although the sample was small, those stars showing the excess polarization had shorter values of λ_{max} (≤ 5100 Å). Clayton et al. (1992) did not observe a position angle rotation in any of the polarization standard stars they measured.

For BD +64°106, $P_{max} \approx 5.67\%$ and $\lambda_{max} \approx 5015$ Å. Allen et al. (1993) measured BD +64°106 during the Science Verification Commissioning Phase of *HST*. Our data is consistent with these earlier results, including the mild rise in the position angle toward shorter wavelengths.

TABLE 2

HST OBSERVATIONAL MODE FOR AG CAR

Epoch	Grating, Waveplate	Aperture	Spectral Range (Å)	Dispersion (Å pixel^{-1})
1991 Nov 19	G270H, Wave B	0.″5	2230–3400	2.5
1992 May 15	G270H, Wave B	1.0	2230–3400	2.5
1992 Jul 16	G270H, Wave B	1.0	2230–3400	2.5

TABLE 3

HST OBSERVATIONS OF BD +64°106

Wavelength (Å)	$\langle P \rangle$ (%)	$\langle \pm\epsilon_P \rangle$	σ_P	ϵ_P/P	$\langle \theta \rangle$	$\langle \pm\epsilon \rangle$	σ_θ
2357.9	3.95	0.35	0.13	0.09	100°9	2°6	1.6
2627.1	4.31	0.20	0.10	0.05	98.5	1.3	1.3
2896.7	4.42	0.16	0.06	0.04	98.9	1.1	0.7
3162.7	4.68	0.17	0.11	0.04	97.9	1.0	1.1

© American Astronomical Society • Provided by the NASA Astrophysics Data System

1994ApJ...428..292L

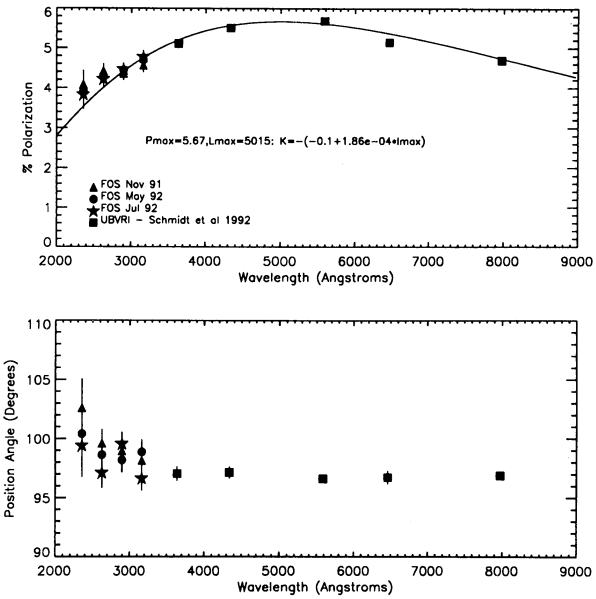

FIG. 2.—Polarization measurements of BD +64°106. Shown are the UV data (averaged into four bins) and the ground-based data (Schmidt, Elston, & Lupie 1992). The UV polarization follows the ISM polarization law. Although the error bars are large, the position angle may be offset by 2°–3° from the optical data. This could represent a real rotation of the ISM plane or a small error in the calibration of the FOS fiducial waveplate position.

2.2. *Ultraviolet Spectroscopy with IUE*

We have used the *International Ultraviolet Explorer* (*IUE*) to obtain both low- and high-dispersion spectra of AG Car, covering the spectral range from 1200 to 2000 Å in the SWP camera and 2000 to 3200 Å in the LWP camera. Low-dispersion spectra achieve a resolution of ~6 Å; a velocity resolution of ~20 km s^{-1} is normally obtained in the high-dispersion mode. Further details on the satellite and its spectrographs can be found in Boggess et al. (1978).

The data were reduced using the standard spectral image processing scheme currently in place at Goddard. The echelle blaze correction is based on the data of Grady & Garhart (1988) for the SWP camera and Ake (1981, 1982) for the long-wavelength cameras. The spectral orders were merged to form single arrays of wavelengths, fluxes, and data quality flags. The fluxes were subsequently calibrated using the calibration tables of Cassatella et al. (1990).

In addition to the spectra obtained within a few days of the *HST*/FOS observations, the *IUE* archives contain a significant number of previous observations of AG Car, spanning a time period of almost 15 yr (see Table 4). In this paper we shall concentrate on the observed variability of the *IUE* spectra as it relates to the problem of determining the outflow characteristics of the wind. The reader is referred to Johnson (1982) for a discussion of the high-dispersion observations obtained in 1980, which includes an extensive list of lines appearing in the spectra. A discussion of the UV light curve, based on low- and high-dispersion *IUE* spectra, can be found in Shore, Waxin, & Altner (1994).

2.3. *Ground-based Spectroscopy*

Spectroscopic data of AG Car in the visual range have been obtained at the 1.6 m telescope of the Brazilian National Observatory (LNA). The spectrograph at the coudé focus was equipped with a coated GEC CCD detector having useable spectral response from 4000–11000 Å. Gratings of 1800 lines mm^{-1} and 600 lines mm^{-1} yielded a dispersion of 0.13 and 0.39 Å $pixel^{-1}$, respectively. The effective spectral resolution as measured from the FWHM of the comparison spectrum is slightly less than 2 pixels. The spectra were reduced in the standard way, Doppler corrected into the heliocentric system, and the continuum was normalized to unity. A summary of all spectra obtained in the course of our observing campaign can be found in Table 5.

In addition to the observations collected in Brazil, we secured several high-resolution spectrograms at the 1.4 m CAT of ESO, La Silla. These observations have a spectral resolution of 60,000. The spectral range is ~50 Å. The spectra are mostly centered on Hα but data for Hβ and He II λ4686 were also obtained. The observing log is also included in Table 5. Standard reduction techniques were performed.

The relatively narrow spectral range made it difficult to normalize the spectra obtained at ESO to the continuum level. Hα in particular has very broad line wings which extend beyond the limits of the accessible spectral region. This problem did not occur on the spectra obtained at LNA due to the much wider spectral range. Since we always had an LNA spectrum within a few weeks of an ESO spectrum, we used the LNA spectra to determine the level of the continuum at the wavelengths where the ESO spectra cut off. The ESO spectra were corrected and normalized to unity with this information.

Some of the spectra obtained at the two observatories differ in spectral resolution by about a factor of 4. We convolved the ESO data with a Gaussian filter to simulate a degraded resolution appropriate for some of the LNA data. Broad emission lines, such as Hα, are still well resolved even on the lowest resolution spectra in our data set. On the other hand, narrow features, such as blueshifted Hα absorption components are strongly affected by instrumental resolution.

The ground-based spectroscopic data cover the spectral evolution of AG Car at a time resolution of a few months. This corresponds to the flow timescale in the wind, which determines the timescale over which the wind features are expected to exhibit significant variations. Since the main thrust of this study is to learn more about the physics of the stellar wind, we concentrated our spectroscopic efforts on obtaining nearly continuous coverage of Hα, the strongest wind line, at the expense of the blue spectral region.

3. POLARIMETRIC PROPERTIES OF AG CARINAE

Is the mass loss from AG Car spherically symmetric, and if not what is the nature of the asymmetry? Spectropolarimetry is an important diagnostic tool for assessing the symmetry of AG Car's stellar wind. The UV regime is advantageous for the following reasons: (1) The contaminating interstellar (ISM) polarization is smaller in the UV, providing us with a better chance to separate the intrinsic and interstellar components of the polarization. (2) The strongest lines formed in the stellar wind (resonance lines of singly ionized iron and magnesium) are found in the UV. (3) Polarization data over an extended wavelength regime (near-simultaneous observations in the UV, optical, and IR) facilitates the characterization of any intrinsic component. The *HST* UV data allow us to probe for asymmetric ejecta in the innermost unresolved region of the complex, without contamination by nebulosity.

The *HST* polarization data for AG Car are presented in

© American Astronomical Society • Provided by the NASA Astrophysics Data System

1994ApJ...428..292L

TABLE 4

JOURNAL OF *IUE* OBSERVATIONS

JD-2,400,000 (1)	Epoch (2)	Symbol (3)	Camera (4)	Image Number (5)	Dispersion (6)	Exposure (s) (7)
44356.....	1980 Apr 27	A	LWR	7628	H	2400
44551.....	1980 Nov 8	B	LWR	9259	H	1920
44819.....	1981 Aug 3	C	LWR	11229	H	1800
44356.....	1980 Apr 27	A	LWR	7627	L	50
44551.....	1980 Nov 8	B	LWR	9258	L	40
45818.....	1984 Apr 28	D	LWP	3236	H	1740
46265.....	1985 Jul 19	E	LWP	6437	H	2640
46383.....	1985 Nov 14	F	LWP	7099	H	1800
46604.....	1986 Jun 23	G	LWP	8469	H	3600
46887.....	1987 Apr 2	H	LWP	10473	H	2700
47000.....	1987 Jul 24	I	LWP	11273	H	2700
47883.....	1989 Dec 23	J	LWP	16985	H	2700
48576.....	1991 Nov 16	K	LWP	21757	H	1800
48577.....	1991 Nov 17	L	LWP	21759	H	900
48760.....	1992 May 18	M	LWP	23126	H	1800
48760.....	1992 May 18	N	LWP	23130	H	2100
48818.....	1992 Jul 15	O	LWP	23508	H	1200
46604.....	1986 Jun 23	G	LWP	8468	L	300
46913.....	1987 Apr 28	...	LWP	10659	L	30
47001.....	1987 Jul 25	I	LWP	11275	L	40
48110.....	1990 Aug 7	...	LWP	18539	L	45
48760.....	1992 May 18	M	LWP	23127	L	30
44551.....	1980 Nov 8	B	SWP	10561	H	7440
44829.....	1981 Aug 13	C	SWP	14750	H	5400
45567.....	1983 Aug 21	α	SWP	20742	H	10800
45845.....	1984 May 25	β	SWP	23109	H	12000
46265.....	1985 Jul 19	E	SWP	26444	H	10800
46604.....	1986 Jun 23	G	SWP	28536	H	10800
47000.....	1987 Jul 24	I	SWP	31405	H	8100
47883.....	1989 Dec 23	J	SWP	37882	H	23400
48576.....	1991 Nov 16	K	SWP	43124	H	7200
48760.....	1992 May 18	M	SWP	44713	H	7200
48818.....	1992 Jul 15	O	SWP	45145	H	7200
43848.....	1978 Dec 6	...	SWP	3542	L	80
44551.....	1980 Nov 8	B	SWP	10560	L	240
44819.....	1981 Aug 3	...	SWP	14639	L	240
45491.....	1983 Jun 6	...	SWP	20157	L	240
45846.....	1984 May 26	β	SWP	23110	L	240
46268.....	1985 Jul 22	E	SWP	26458	L	180
46383.....	1985 Nov 14	...	SWP	27111	L	180
46604.....	1986 Jun 23	G	SWP	28537	L	180
46887.....	1987 Apr 2	H	SWP	30691	L	180
46913.....	1987 Apr 28	...	SWP	30881	L	90
47151.....	1987 Dec 22	...	SWP	32588	L	180
47583.....	1989 Feb 26	...	SWP	35625	L	180
48011.....	1990 Apr 30	...	SWP	38703	L	240
48576.....	1991 Nov 16	K	SWP	43123	L	240
48760.....	1992 May 18	M	SWP	44710	L	240
48818.....	1992 Jul 15	O	SWP	45144	L	240

NOTES.—The symbols "α" and "β" in col. (3) refer to epochs in which only SWP spectra were obtained.

Figure 3 where we have displayed the relative flux, and the polarization and position angle for all 3 epochs of observations. The error bars in this figure indicate the 1 σ errors. According to our *IUE* monitoring, the dominant spectral features did not vary over the course of our *HST* observations. The prevalent feature in the polarization is the decrease by 0.5% in 1992 May from the 1991 November level, followed by a return in 1992 July to the higher polarization state. The position angle is constant with wavelength and shows a small rotation between 1992 May and 1992 July. The errors are large on the May position angle data because the polarization is so low. We also acquired ground-based polarization data with IAGPOL at the 0.6 m and 1.6 m telescopes of the Brazilian National Observatory on 1991 June 3 and on 1992 May 1. These data are presented in Table 6.

Polarization measurements are very sensitive to asymmetries but quantitative interpretation is made difficult by the presence of interstellar polarization, which is often not known, and possibly by competing intrinsic polarization from different origins (e.g., a variable component superimposed on a constant component). Three methods are used to detect the presence of an intrinsic component: (1) a wavelength dependence that is different from the interstellar law, (2) variability, and (3) polarization structure across absorption/emission lines.

© American Astronomical Society • Provided by the NASA Astrophysics Data System

1994ApJ...428..292L

TABLE 5

JOURNAL OF GROUND-BASED SPECTROSCOPIC OBSERVATIONS

Epoch (1)	Telescope (2)	Spectral Range (Å) (3)	Dispersion (Å/pixel^{-1}) (4)
1990 Jun 16	LNA	9950–10190	0.4
1990 Dec 22	LNA	9960–10190	0.4
1990 Dec 27	LNA	8600–8830	0.4
1990 Dec 28	LNA	6490–6714	0.4
1991 Jan 21	ESO	4670–4720	0.05
1991 May 25	LNA	10740–10960	0.4
1991 Jul 31	ESO	6540–6590	0.05
1991 Aug 15	LNA	6500–6730	0.4
	LNA	8580–8800	0.4
	LNA	9950–10170	0.4
1991 Oct 22	LNA	6380–6850	0.4
	LNA	8460–8940	0.4
1991 Nov 18	LNA	6490–6640	0.1
1991 Nov 25	LNA	6600–6750	0.1
1992 Jan 3	ESO	6530–6590	0.05
1992 Mar 17	ESO	6530–6590	0.05
1992 Mar 19	ESO	4840–4880	0.05
1992 Mar 20	LNA	6410–6880	0.4
	LNA	8480–8950	0.4
	LNA	9940–10410	0.4
	LNA	10570–11040	0.4
1992 May 15	ESO	6530–6590	0.05
1992 Jun 3	LNA	4170–5100	0.4
	LNA	5790–6260	0.4
	LNA	6380–6850	0.4
	LNA	8400–8900	0.4

3.1. *Interstellar Polarization of AG Car and Surrounding Field Stars*

The measured polarization is a vector combination of the intrinsic polarization of the star and the interstellar polarization. At this time, we do not know, with sufficient accuracy the interstellar vector toward AG Car. An estimate can be made using polarization measurements of neighboring stars from the catalog of Klare, Neckel, & Schnur (1972) which contains the (effective) *B* filter polarization of southern stars. The results of the search at distances of (6 ± 3) kpc are given in Table 7 where DM is the distance modulus, δDM is the depth of the region. The rms deviation of P and θ are also given. The projected area on the sky is 1°. From the 6 kpc data, the interstellar position angle is 135° with a ±5° uncertainty. From SMF, λ_{max} determined from stars in the *general* area of AG Car is between 5200 and 5700 Å. Using a mean value of $P(B) = 1\%$ at 6 kpc (DM = 13.9) and the Wilking et al. (1982) modification of SMFs formulation, $P_{max} \approx 1.0\%$ and 1.1% using $\lambda_{max} = 5200$ and 5700 Å, respectively.

TABLE 6

RECENT GROUND-BASED PHOTOPOLARIMETRY OF AG CAR

Epoch	Wavelength (Å)	P[a] (%)	θ[b]
1991 Jun 3	3620	0.79 (0.07)	133°.8 (2°.4)
	4506	1.01 (0.05)	134.1 (1.3)
	5445	1.15 (0.06)	133.8 (1.4)
	6519	1.34 (0.05)	134.5 (1.1)
	7975	1.41 (0.06)	132.6 (1.2)
1992 May 2	5445	1.14 (0.11)	148.2 (2.7)
	6519	1.19 (0.09)	151.9 (2.2)
	7975	0.94 (0.17)	145.1 (5.1)

[a] Numbers in parentheses are percentages of errors.
[b] Numbers in parentheses are errors, in degrees.

TABLE 7

POLARIZATION OF NEARBY STARS

DM	δDM	Number	$\%P(B)$	$\theta(B)$
13.9	1	14	1.1 ± 0.2	141° ± 4°
13.9	2	40	0.8 ± 0.3	131 ± 4
12.4	1	40	0.8 ± 0.3	126 ± 3
12.4	2	51	0.8 ± 0.3	127 ± 3
14.8[a]	1	10	1.0 ± 0.3	135 ± 3
14.8	2	15	1.1 ± 0.2	140 ± 3

[a] 2° search area. All others are 1°.

Schulte-Ladbeck, Clayton, & Meade (1993) estimated the interstellar polarization toward AG Car by measuring the polarization across the Hα emission line. If one can assume that the line is unpolarized, a result of seeing less scattering optical depth than the continuum, the polarization at the core represents the interstellar value at 6563 Å. This method is exceedingly more preferable than using neighboring stars. However, the assumption that the line is *totally* unpolarized requires independent confirmation. If the line is unpolarized, then the P_{max} values derived from the Hα data are 1.25% and 1.20% for $\lambda_{max} = 5200$ Å and 5700 Å, respectively, and the position angle is 143°. Both the polarization and position angle slightly exceed the envelope of estimates from neighboring stars.

The polarization and position angle history of AG Car is presented in Figure 4 as a function of wavelength. Here we access measurements obtained by Serkowski (1970) over a 511 day period (1968 February and April, 1969 February–June). The *HST* UV data are displayed in eight bins (150 Å per bin). The Brazil optical data and an optical spectropolarimetric continuum measurement (~6500 Å in 1991 November from Schulte-Ladbeck, Clayton, & Meade 1993) are also shown. The aperture sizes used for ground-based photopolarimetric measurements are 20″ and 30″, significantly larger than our 0.″5 and 1″ apertures used for the UV data. These larger apertures encompass the entire AG Car complex. Schulte-Ladbeck et al.'s data was obtained with a 2.″7 aperture. The data obtained on the same date are connected with a *dashed* line and the data obtained within a month are connected with *dotted* lines. The solid curve is an estimate of the interstellar polarization using the stars from the Klare et al. catalog ($\lambda_{max} = 5500$ Å, $P_{max} = 1\%$). We note that the envelope of uncertainty would outline a swathe many tenths of an arcsecond wide.

A fit using all the AG Car optical data resulted in $\lambda_{max} \approx 6900$ Å. Fitting the interstellar law to a star with variable polarization is only meaningful in that it shows qualitatively that the wavelength dependence is different from the interstellar medium. The position angle is constant with wavelength in the optical whereas the UV shows a rotation of ~10° (cf., 1991 November, UV + optical).

3.2. *Polarization Variability*

Any variation seen in the polarization with time is intrinsic to the star or its immediate surroundings. The variability is a lower limit on the magnitude of the intrinsic component. Table 8 summarizes the polarization variability of AG Car. Columns (1) and (2) list the wavelength and number of visits, columns (3)–(6) and (7)–(10) give the mean, standard deviation, average

© American Astronomical Society • Provided by the NASA Astrophysics Data System

1994ApJ...428..292L

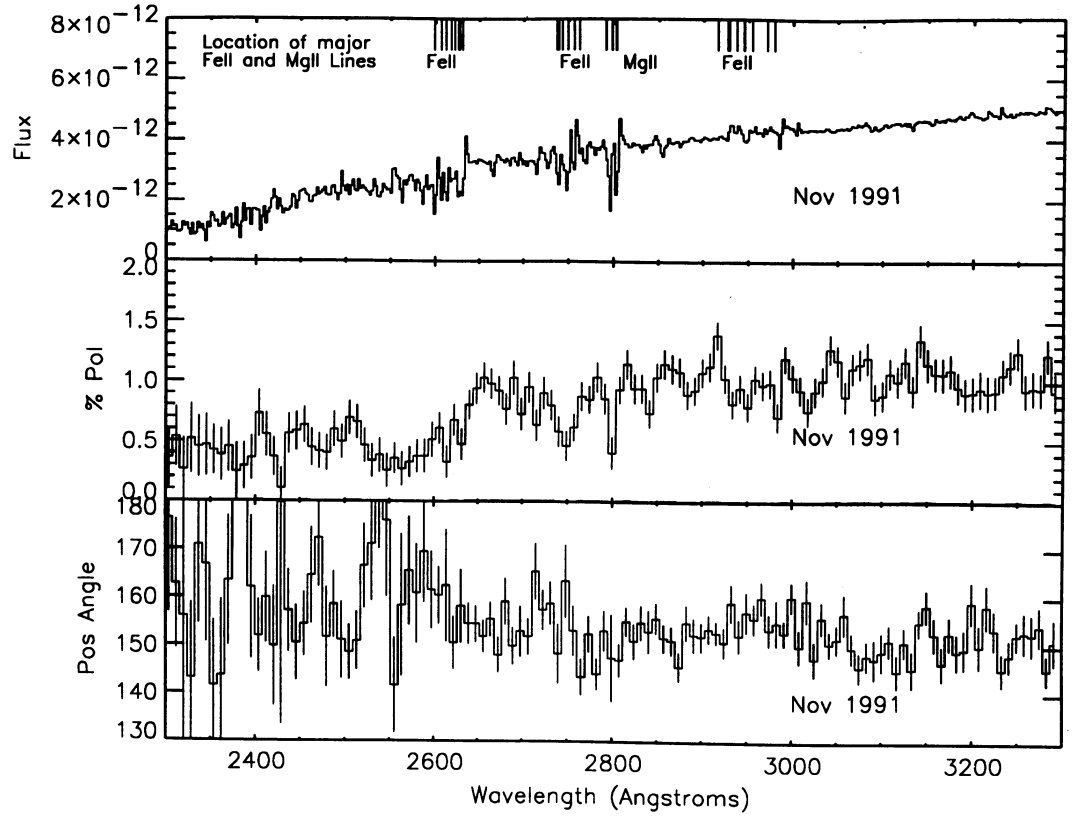

FIG. 3*a*

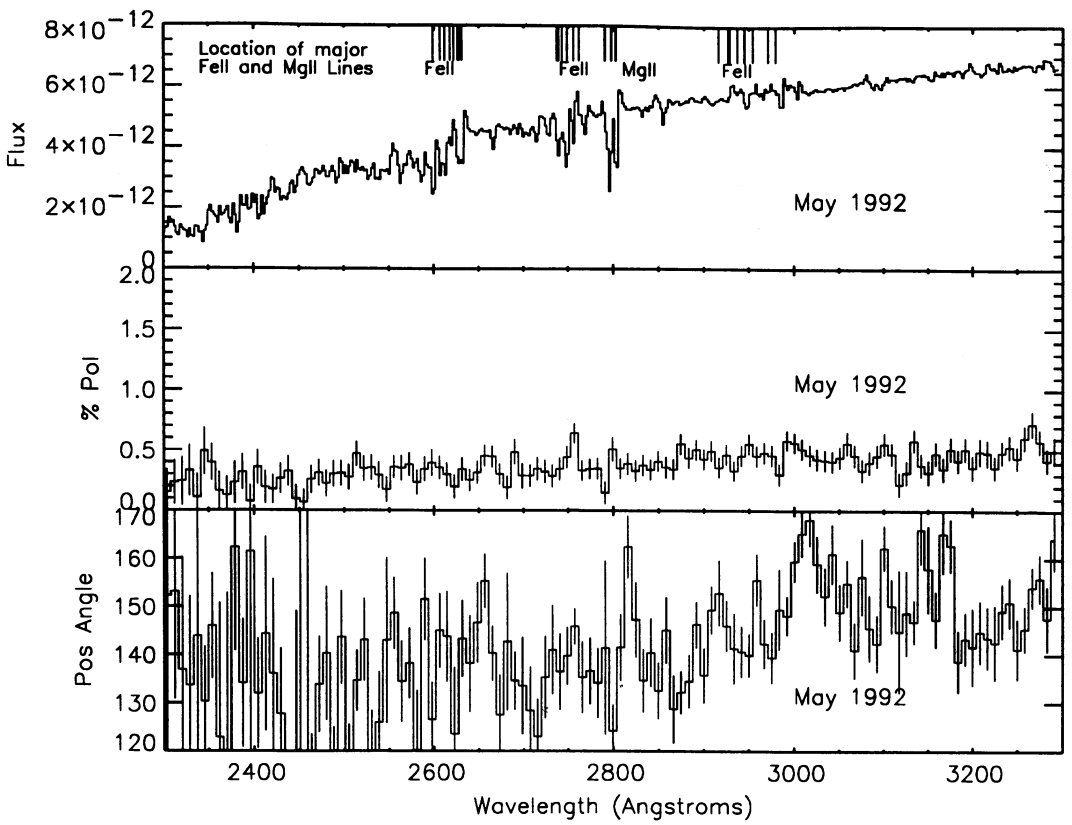

FIG. 3*b*

FIG. 3.—*HST* FOS spectra and polarimetry. Presented here are flux, polarization, and position angle for the (*a*) 1991 November, (*b*) 1992 May, and (*c*) July 1992 FOS spectra. The UV data are displayed in 10 Å bins. The continuum polarization decreases by 0.5% in 1992 May and recovers in 1992 July. Some of the structure seen across the P Cygni lines is a result of saturated absorption and our limited wavelength resolution which causes mixing of the continuum and line fluxes.

© American Astronomical Society • Provided by the NASA Astrophysics Data System

1994ApJ...428..292L

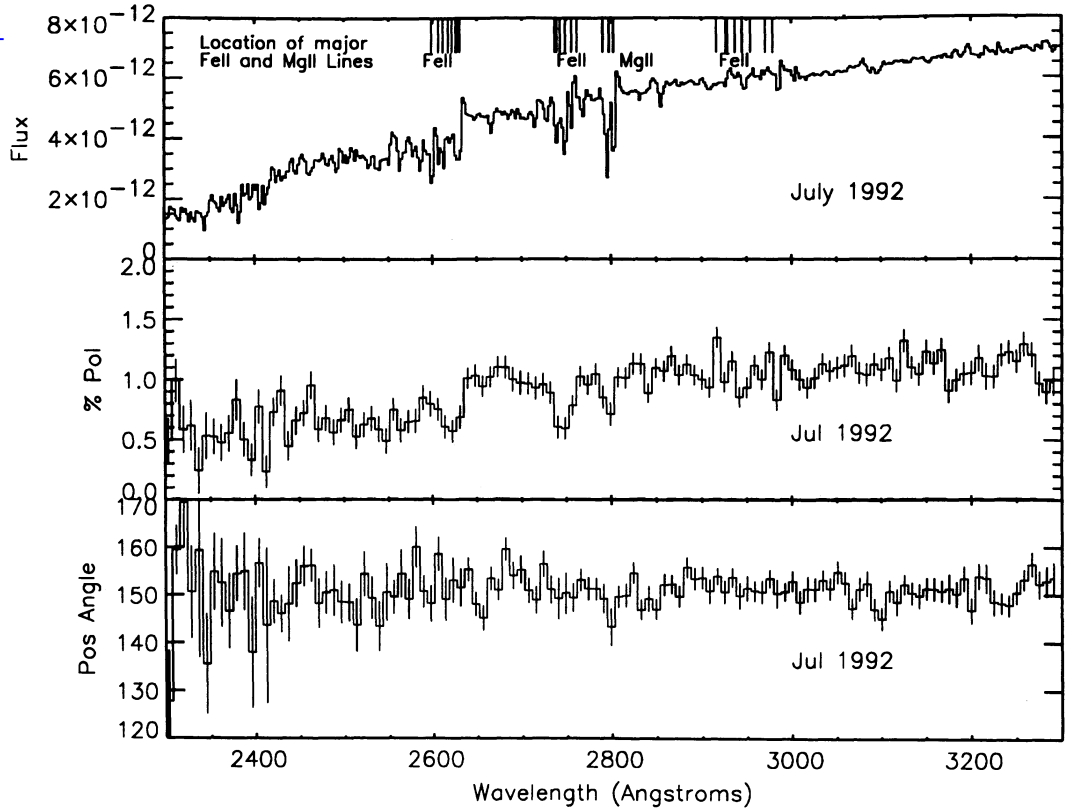

FIG. 3c

TABLE 8

SUMMARY OF AG CARINAE POLARIZATION

Band (1)	Visits (2)	$\langle P \rangle$ (%) (3)	σ_P (%) (4)	$\langle$err$\rangle$ (%) (5)	max δP (%) (6)	$\langle \theta \rangle$ (7)	σ_θ (8)	$\langle$err$\rangle$ (9)	max $\delta\theta$ (10)
Serkowski 1968–1970									
U	4	0.81	0.12	0.06	0.29	141°2	3°5	2°0	9°0
B	8	0.97	0.15	0.06	0.51	138.3	4.0	1.7	13.0
V	3	1.21	0.13	0.06	0.32	137.8	3.2	1.4	7.0
Brazil 1991–1992									
U	1	0.79	...	0.07	...	133.8	...	2.4	...
B	1	1.01	...	0.05	...	134.1	...	1.3	...
V	2	1.15	0.01	0.09	0.01	136.9	8.3	2.0	14.4
R	2	1.31	0.09	0.09	0.16	138.0	10.2	1.7	17.4
I	2	1.36	0.30	0.12	0.47	133.2	8.4	3.2	12.5
HST UV Data (150 Å bins) 1991–1992									
2291	3	0.43	0.16	0.06	0.39	154.2	9.4	4.6	21.8
2425	3	0.41	0.18	0.04	0.45	151.0	15.1	3.1	32.9
2560	3	0.47	0.15	0.03	0.35	150.1	9.7	2.0	23.1
2694	3	0.67	0.24	0.03	0.56	151.5	7.2	1.3	15.3
2829	3	0.75	0.29	0.03	0.66	149.9	6.8	1.1	12.8
2963	3	0.79	0.28	0.03	0.61	152.2	2.0	1.0	4.7
3096	3	0.84	0.32	0.02	0.71	150.8	0.6	1.0	1.1
3229	3	0.83	0.28	0.03	0.62	151.0	1.0	1.1	1.8

© American Astronomical Society • Provided by the NASA Astrophysics Data System

1994ApJ...428..292L

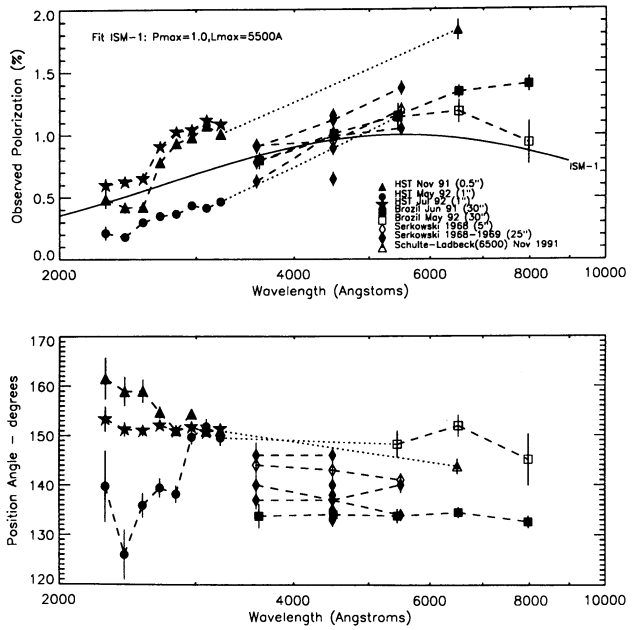

FIG. 4.—Polarization history of AG Car. The UV data is presented in bins of 150 Å. We have included data from Serkowski (1970), Schulte-Ladbeck (1993), and our 1991–1992 optical + UV data as indicated in the key. Data taken on the same date are connected by dashed lines and data taken within a month are connected by dots. The solid line represents a crude estimate of the interstellar polarization derived from nearby stars (see text for discussion).

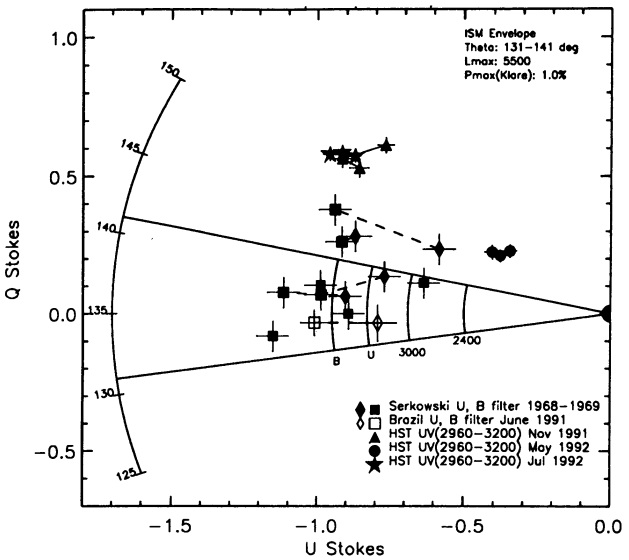

FIG. 5.—Temporal variability of AG Car in the $Q-U$ plane over a limited wavelength range. Displayed are the U and B Serkowski data (1968–1969), the Brazil U and B data (1991 June), and the red end (2900–3200) of the *HST* UV data (binned to 150 Å). *Dashes* connect points on the same date, and *filled circles* connect data obtained within a month. The (0, 0) position on the graph is denoted by a bull's eye. We have also shown the interstellar polarization envelope and our arcs which represent an estimate of the magnitude of the interstellar polarization at four wavelengths (using $P_{max} \approx 1\%$, $\lambda_{max} \approx 5500$ Å, $\theta = 135°$).

(typical) error, and maximum change for the measured polarization and position angle, respectively.

In summary, Serkowski has seen variability of ~0.5% over a few months time, Brazil I data varies by ~0.4% in 11 months, the UV 1991 November and 1992 July data are very similar but the intervening 1992 May data falls to less than 0.5%, resulting in a change in polarization of ~0.6%. This small polarization observed in May is *consistent* with the polarization seen by Schulte-Ladbeck (1993, private communication) in the optical continuum a few months earlier, in 1992 March [$P(5500) \approx (0.85 \pm 0.08)\%$, $\theta \approx 145°$]. The timescale of variability is not established but dramatic 0.5% changes in the polarization are seen over a period of 1–2 months.

Presentation of the data on the $Q-U$ plane reveals additional information about the nature of the variable intrinsic component. The polarization data is displayed on the Stokes $Q-U$ plane in Figures 5 and 6. The length of the vector on a $Q-U$ plane is equal to the magnitude of the polarization (intrinsic + interstellar) and a rotation on the $Q-U$ plane is equal to half that value on the plane of the sky. Let us first confine the input to data in *one wavelength regime*. Figure 5 displays the polarization in U, B and the long-wavelength end of the *HST* UV data (2900–3200 Å). The (0, 0) position on the graph is denoted by a bull's eye. We have also shown the interstellar polarization envelope and four arcs which represent the magnitude of the interstellar polarization at four wavelengths (using $P_{max} \approx 1\%$, $\lambda_{max} \approx 5500$ Å, $\theta = 135°$). If the intrinsic polarization is produced by a constant scattering plane, such as an axisymmetric disk (Be stars) or a stable localized region, the measured points (which are a combination of intrinsic and interstellar) would aggregate along a preferred direction, or "time path." If the points aggregated into a circular or elliptical distribution which is repeatable in time, the variability is caused by a periodic phenomenon such as a companion star in a binary system. If the intrinsic position angle varies randomly (such as blobs emitted from many latitudes), one would expect a random pattern clustered around the tip of the interstellar vector. We would expect changes in the polarization also as a result of the outward motion of the blob. Fox & Henrichs (1994) followed the polarization path of a parcel

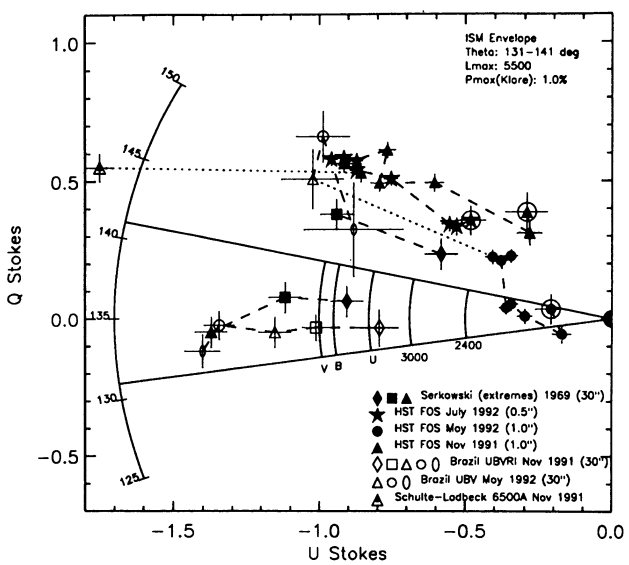

FIG. 6.—AG Car wavelength dependence on the $Q-U$ plane. The observed polarization at several different wavelengths is shown. The two most extreme points from Serkowski (1970) are included. Data obtained on the same date are connected by *dashes* and data obtained within the same month are connected by *filled circles*. It is important to address the multiwavelength data taken at the same time in this diagram. If we adopt the estimate of the interstellar component shown by the arcs, it is clear that there are times when the intrinsic polarization wavelength dependence, and to a lesser extent, the magnitude of the position angle also varies with wavelength.

© American Astronomical Society • Provided by the NASA Astrophysics Data System

1994ApJ...428..292L

ejected from a hot star for various combinations of density, inclination angle, and location on the star. As the parcel moves out, the intrinsic component reaches a peak, then decreases. The intrinsic position angle changes as well and flattens out, a result of the aspect angle.

The paucity of points in Figure 5 and the irregular sampling time precludes any assessment of periodicity, or sampling of parcel motion. Even so, a clear-cut "pattern" is not readily revealed. If the interstellar polarization vector falls somewhere within the distribution of points, one might conclude that the intrinsic position angle sometimes has a value of $\sim 5°$ (points falling above the line) and 100° (falling below the line), corresponding to a 90° rotation of the plane of scattering.

Figure 6 is a $Q-U$ diagram which displays the polarization at several different wavelengths but *at approximately the same epoch.* Data obtained on the same date are connected by dashes, and data obtained within the same month are connected by dots. The *HST* UV data are displayed in eight bins (150 Å per bin) as before but the shortest wavelength bin is circled in the figure. Symbols for the other data points are described in the key. It is important to address the multiwavelength data taken at the same time in this diagram. We will assume that the interstellar position angle is wavelength independent. (If multiple interstellar clouds with different properties lie along the sight line, a rotation of θ is possible). If we adopt the estimate of the interstellar component shown by the arcs, it is clear that there are times when the intrinsic position angle has a wavelength dependence, and to a lesser extent, the magnitude of the intrinsic component also varies with wavelength.

3.3. *Polarization Structure across UV P Cygni Lines*

The interstellar polarization is a smoothly varying function with wavelength and has a constant or linear slope across stellar line profiles. Polarization line structure can provide a method to compare the geometry of the line-forming regions with continuum polarization sources.

Polarization and position angle variations across emission lines were first observed in Be stars (e.g., Capps, Coyne, & Dyck 1973; Clarke & McLean 1974) and in the Wolf-Rayet star HD 50896 (McLean et al. 1979). Schulte-Ladbeck, Clayton, & Meade (1993) have measured changes in the polarization across AG Car's Hα line. In the case of the Hα emission line, the region producing the emission sees a smaller electron scattering optical depth than the photospheric light. The addition of the unpolarized emission dilutes the intrinsic polarization at line center and, if the dilution is complete, only the interstellar component will remain at line center. The interstellar and intrinsic contributions add vectorally, hence the position angle may vary across the line as the dominating polarization changes from intrinsic to interstellar. The polarization across P Cygni resonance lines of supernovae is discussed in McCall (1984) and, with, the combined effects of the interstellar polarization is expected to be a complex function.

Our resolution is not sufficient to sample the wings of the strong P Cygni lines without mixing of the local continuum and absorption troughs. An example of a line with an unsaturated core is Fe II (78) at 2985 Å. We see marginal polarization structure across the line if we average together the November and July values. This is reasonable since the polarization in this region has not changed significantly. We are currently in the process of a statistical evaluation of the shapes of all the UV lines (saturated and not) in P and θ and a comparison with the shapes derived from convolving the FOS instrument profile with the *IUE* data. At the least, we hope to qualitatively determine whether the UV resonance lines are polarized differently than the UV continuum light (Lupie 1994).

3.4. *Wavelength Dependence of the Intrinsic Polarization*

The features seen in the UV polarization (1991 November and 1992 July; Fig. 3) include a reduction in the polarization around 2600 Å, structure in the polarization across the strongest Fe II and Mg II resonance lines and a general slope toward longer wavelengths, the latter of which is in part due to the contribution by the interstellar vector. A drop in the polarization has also been seen in the WUPPE UV data for P Cygni (Taylor et al. 1991). In both P Cyg and AG Car, there are many Fe II P Cygni lines in this region. Taylor et al. (1991) speculated that the reduction in the polarization is probably due to line blanketing and that polarization models for these stars should include the absorptive opacity from heavier elements. In our case, our limited wavelength resolution combined with the extensive number of these saturated lines contributes at least in part to the apparent drop in polarization at 2600 Å and similarly across the saturated Fe II and Mg II lines throughout the spectrum.

The intrinsic behavior can be seen in Figures 7 and 8 which display intrinsic polarization and position angle, i.e., the reslting polarization after an assumed interstellar component has been removed. The errors on the points are simply the observational error and do *not* include the uncertainty in the placement of the interstellar vector. In Figure 7, we used the interstellar polarization estimated for nearby stars and adopted the mean value for $\lambda_{max} = 5500$ Å, $P_{max} = 1\%$, and $\theta = 135°$. The results indicate increase in polarization with wavelength by 0.2%–0.4% at least some of the time. The intrinsic position angle for 1991 November and 1992 May shows a 30° rotation from the UV to the optical.

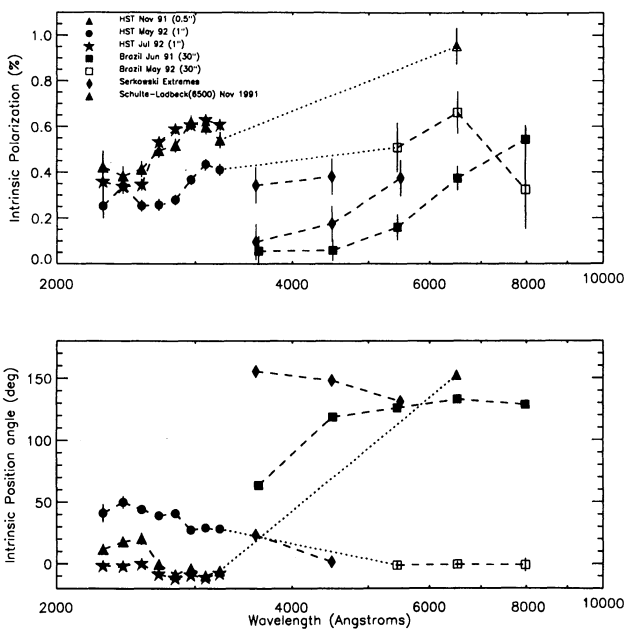

FIG. 7.—AG Car intrinsic polarization using a model for the interstellar component that is based on nearby stars, extracted from the catalog of Klare, Neckel, & Schnur (1972). Note that the nearby stars exhibit a 10° range in position angle and a 0.3%–0.4% range in P_{max}.

© American Astronomical Society • Provided by the NASA Astrophysics Data System

1994ApJ...428..292L

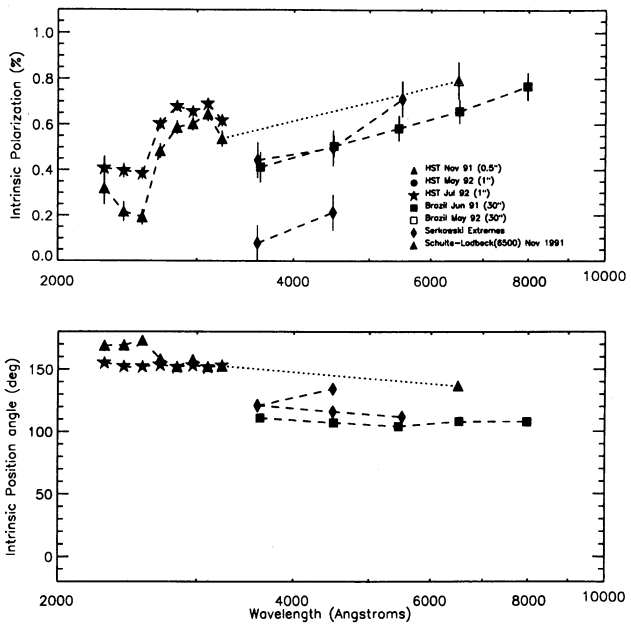

FIG. 8.—AG Car intrinsic polarization using a model for the interstellar component that is based on the 1992 May AG Car data, where the 0.5% drop in polarization suggests that the intrinsic component may have disappeared or have been "cancelled out."

Figure 8 displays the resulting polarization when another model for the interstellar polarization is assumed. Here we adopted a very high value of $\lambda_{max} = 7000$ Å and $P_{max} = 1.1\%$, $\theta = 149°$. These values follow from the assumption that the 1992 May data are not contaminated by any intrinsic polarization, i.e., they are exclusively due to interstellar polarization. The drop in polarization in 1992 May indeed suggests that the component of intrinsic polarization was at a minimum or had disappeared (or was cancelled by changes in the geometrical configuration of asymmetry). Of course, a minimum polarization can be achieved by adding an equal but opposite intrinsic component to the interstellar component. With this model, a 0.2%–0.3% slope is seen in the polarization but the position angle is much flatter.

There are ways to produce a wavelength dependence in the polarization and for this to change as a function of time. Electron scattering polarization is flat with wavelength. McLean (1979) first showed for Be stars that this *flat* polarization could be sculpted by the effects of absorption by hydrogen. In effect the polarization decreases toward the hydrogen series limits. Cassinelli, Nordsieck, & Murison (1987) confirmed that this polarization wavelength dependence can be generated by plumes in hot stars. Taylor & Cassinelli (1992) addressed the polarization wavelength dependence for a two-component (disk + plume) model. In this model, the wavelength dependence for a pole + plume-dominated polarization was shown to have an opposite effect than a disk-dominated polarization, i.e., rather than decreasing as the polarization approaches the series limits, the polarization can show an increase. The contribution from circumstellar dust also results in wavelength-dependent polarization which increases toward the UV. However, this effect should be minimal when observations are made with small apertures which address the innermost region of the star complex. The 30° position angle rotation as a function of wavelength that we see in AG Car is more difficult to explain even with the two-component wind model.

In summary, with the data and wavelength regime we have available, we find (1) AG Car has significant polarization. (2) The polarization is variable on a timescale of 2 months or less. (3) There is evidence that the polarization magnitude varies with wavelength and that the position angle also shows a wavelength dependence. Additional monitoring, i.e., simultaneous measurements over large wavelength regimes is essential for a more quantitative interpretation of these results. We propose an axial-symmetric geometry for the outflow with a variable, equatorial-disk-like density enhancement and a less dense polar wind as being consistent with the polarimetric observations. This geometry is quite similar to the wind structure derived from the spectroscopic observations described in § 4.2.

4. PHOTOMETRIC AND SPECTROSCOPIC EVOLUTION

4.1. *Continuum*

Our spectroscopic and spectropolarimetric campaign began in late 1990 when AG Car was in the steep, ascending part of its light curve (cf. Fig. 1). Observations during this period are particularly well suited to investigate relationships between the wind properties and the rapidly changing photospheric parameters since the spectral types range from late-O to about B2 during this time. In contrast, the only detailed wind analysis of AG Car published so far (Wolf & Stahl 1982) was done when AG Car was at maximum light around 1982. At that time, AG Car had an equivalent spectral type of early-A. If the light curve is extrapolated into the future, we would expect AG Car to reach a state similar to the one observed by Wolf & Stahl (1982) sometime in 1994/1995.

As a word of caution, the apparent periodicity implied by Figure 1 may be misleading. Comparison with light curves from earlier epochs (Mayall 1969) shows that the regular photometric behavior of AG Car over the last 15 yr is exceptional. The light curves obtained at earlier epochs during this century are much more irregular although part of the difference may be due to improved measurement techniques.

Superposed on the broad minimum between 1985 and 1990 are variations on a smaller scale with amplitudes of up to 0.3 mag. (Similar variations may also be present in the ascending and descending parts of the light curve but they would be more difficult to detect.) We performed a period analysis for the epoch 1985.0 until 1991.0, using the phase dispersion minimization algorithm within IRAF (Stellingwerf 1978). The most significant periods are 1.0 yr and multiples of this value. The most likely interpretation is one of observational bias. Observing conditions are strongly dependent on the observing season, in particular if the observations are done visually. This explanation seems even more likely considering that the largest scatter around the mean light curve occurs predominantly in the second half of each year when AG Car is close to the Sun and difficult to observe. We do not challenge the existence of the so-called "microvariations" (van Genderen et al. 1988), which occur on a timescale of days to weeks, with an amplitude smaller than the one discernible in Figure 1: typically 0.1 mag or less.

Viotti et al. (1984) first demonstrated that the brightness variations of AG Car in the visual are anticorrelated with the ultraviolet variability. Subsequently Lamers et al. (1989) refined the analysis of Viotti et al. and showed that the bolometric luminosity remains constant at $\log L/L_{\odot} = 6.2 \pm 0.2$ during an activity cycle, and that $E(B-V) = 0.63 \pm 0.02$. We

© American Astronomical Society • Provided by the NASA Astrophysics Data System

1994ApJ...428..292L

used all available low-dispersion ultraviolet observations of AG Car from the *IUE* archive (see Table 4) to determine the bolometric luminosity. The *IUE* data were combined with existing visual and near-infrared (Whitelock et al. 1983) photometry. We found that L = constant if $E(B-V) = 0.63$, in agreement with Lamers et al. (1989). Our somewhat more complete data set resulted in a luminosity which is slightly lower but still consistent with the one found by Lamers et al.: $\log L/L_{\odot} = 6.0 \pm 0.2$. A distance of (6 ± 1) kpc was adopted (Humphreys et al. 1989).

4.2. *Ultraviolet Lines*

A montage of selected *IUE* high-dispersion obtained between 1980 and 1992 is shown in Figure 9. The variations of the line spectrum reflect the very different photospheric and wind conditions at the various epochs. In comparison with the optical lines, the ultraviolet line spectrum shows less dramatic variations. In particular, few variations are apparent between the epochs of our ground-based and *HST* observing campaign. One reason is that many ultraviolet features originate far out in the wind, with correspondingly long response times to variations in the inner regions. However, we will argue below that the ultraviolet properties of AG Car's wind are indeed different from the optical properties.

Many of the UV P Cygni lines in the *IUE* spectra indicate a terminal wind speed close to the -250 km s^{-1} value obtained from the 1990 December Hα observations (see § 5). We measure -290 km s^{-1} at the steep blue edge in both components of the Mg II resonance doublet ($\lambda\lambda$2795, 2802), and the Al II λ1671 line, with little or no variation over the entire span of observation with *IUE*. All velocities refer to the heliocentric system. Somewhat lower terminal velocities can also be identified (-260 km s^{-1} in Fe II λ2585, -250 to -200 km s^{-1} in Si II λ1808 and Ni II λ1455). For the most part, the majority of the P Cygni features mentioned above have well delineated edges. In general, the smaller terminal velocities also tend to be the most variable, although this is likely due to saturation effects in the strong resonance lines such as Mg II. This variability, coupled with the frequent contamination of profiles with overlapping photospheric lines or other wind lines, makes estimation of reliable velocities somewhat difficult in certain cases, even when the blue edge of the profile is steep (i.e., the Fe II λ2599 resonance line appears to have an edge velocity in excess of -400 km s^{-1}, but this is probably an overestimate caused by the neighboring Fe II λ2598 line). Nevertheless, although the observations do not support a simple linear increase in terminal velocity with decreasing excitation, as suggested by Johnson (1982) and Caputo & Vioti (1970), they are qualitatively consistent with the picture of a wind with the excited state transitions forming near the star, where the wind is densest, and gradually accelerating outward, with the maximum velocity showing up in the ground-state lines.

Several rather remarkable spectral signatures complicate this simple picture of a slow, gradually accelerating, dense wind in AG Car. The first of these relates to what may be called "fine structure" in the unsaturated P Cygni line profiles. This phenomenon was first observed among the Fe II lines in P Cygni by Cassatella et al. (1979) and in AG Car by Johnson (1982). Johnson interpreted the variability of the relative strengths of the doubled absorption features (at -175 and -25 km s^{-1}) as evidence of mass ejection "events"; i.e., shells or puffs ejected at different epochs (spectra A and B in Fig. 9, separated by 194 days) with different accelerations.

Johnson (1982) stressed that the variability of the -25 km s^{-1} feature precluded its being interstellar, and the evidence of 10 more years of observation shows him to have been correct on this point, although there is indeed a very strong interstellar component in the spectral line profiles. For example, the λ2585 ground-state transition of Fe II (multiplet 1) shown in Figure 10 with the full line, includes a broad (125 km s^{-1}) absorption in *every* LWR and LWP spectrum. During the phase of optical minimum, when AG Car was at its hottest (here represented by epoch J), the line is largely due to interstellar absorption, since most of the Fe II is ionized to Fe III (note, however, that the centroid of the feature is offset by about -25 km s^{-1}). The dotted line in each plot shows the P Cygni profile due to the 0.08 eV excited state in Fe II (1) at λ2631.32. Although the IS absorption at zero velocity is clearly absent, as to be expected for an excited state, the absorption at ~ 50 km s^{-1} is definitely variable. Thus, the broad absorption of Fe II λ2585 near rest velocity is undoubtedly a superposition of a true IS component and a variable-strength low-velocity wind line.

At epochs before and after optical minimum a deep P Cygni absorption at higher velocity is also present, extending out to -400 km s^{-1} in the λ2585 resonance line, but only to -300 km s^{-1} in the excited state line. Careful examination of these profiles, and of similar profiles in other lines, reveals multiple weak features, some of which are common to both transitions. As Johnson (1982) pointed out, it is at times difficult to identify such features as photospheric or as wind components. In order to shed further light on this question we show in Figure 11 the superposed line profiles of Fe II λ1608.45 (observed with the SWP camera), and Fe II λ2585.88 (observed with the LWP camera) at eight of the 9 epochs common to both cameras. There appears to be a significant degree of agreement between the two lines, even among the weak absorption features (see especially, epoch K). Both of these are reasonance lines and have almost equal oscillator strengths and both include an interstellar component. But because they were measured in two different cameras, and two entirely different wavelength regions, it is highly unlikely that this correspondence is due to detector systematics (i.e., fixed pattern noise) or photospheric lines. Hence, these features must be real. Further, they suggest that several, perhaps many, distinct shells of gas exist in the wind of AG Car, ejected in different events during the course of evolution of this unstable star and now superposed along our line of sight.

The most conspicuous deviation from the behavior described above is seen in the P Cygni profiles of the Si IV resonance doublet at $\lambda\lambda$1393, 1402 (see Fig. 12). During optical minimum the Si IV lines are much stronger than at other phases, as to be expected for a highly ionized species. But what is most interesting about these lines is the gradual climb back toward the continuum, rather than abrupt edge seen in most other lines, and the large velocity of the bluest features identifiable with this flow (-900 to -1000 km s^{-1}). The superposition of the doublets profiles in Figure 12 lends credibility to the claim that the wind really does extend to such a high velocity in Si IV and is not merely attributable to contamination by other lines or by photospheric Si IV. Some contamination by the broad wings of photospheric Si IV may contribute to the broadening of the profile when AG Car was at its hottest. However, it seems unlikely that this could be the case when AG Car was later than spectral type early B. Further, close inspection of Figure 12 suggests that here too fine structure may be present, reminiscent of discrete absorp-

© American Astronomical Society • Provided by the NASA Astrophysics Data System

1994ApJ...428..292L

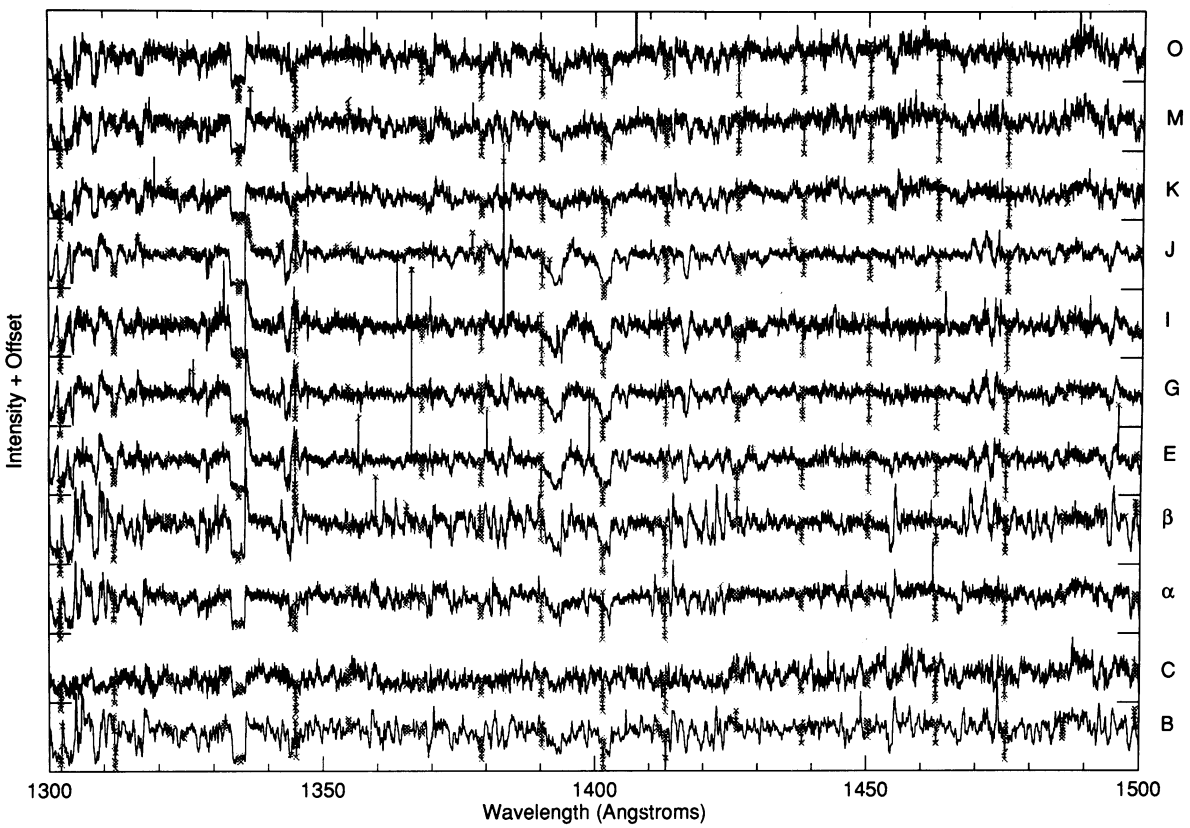

FIG. 9*a*

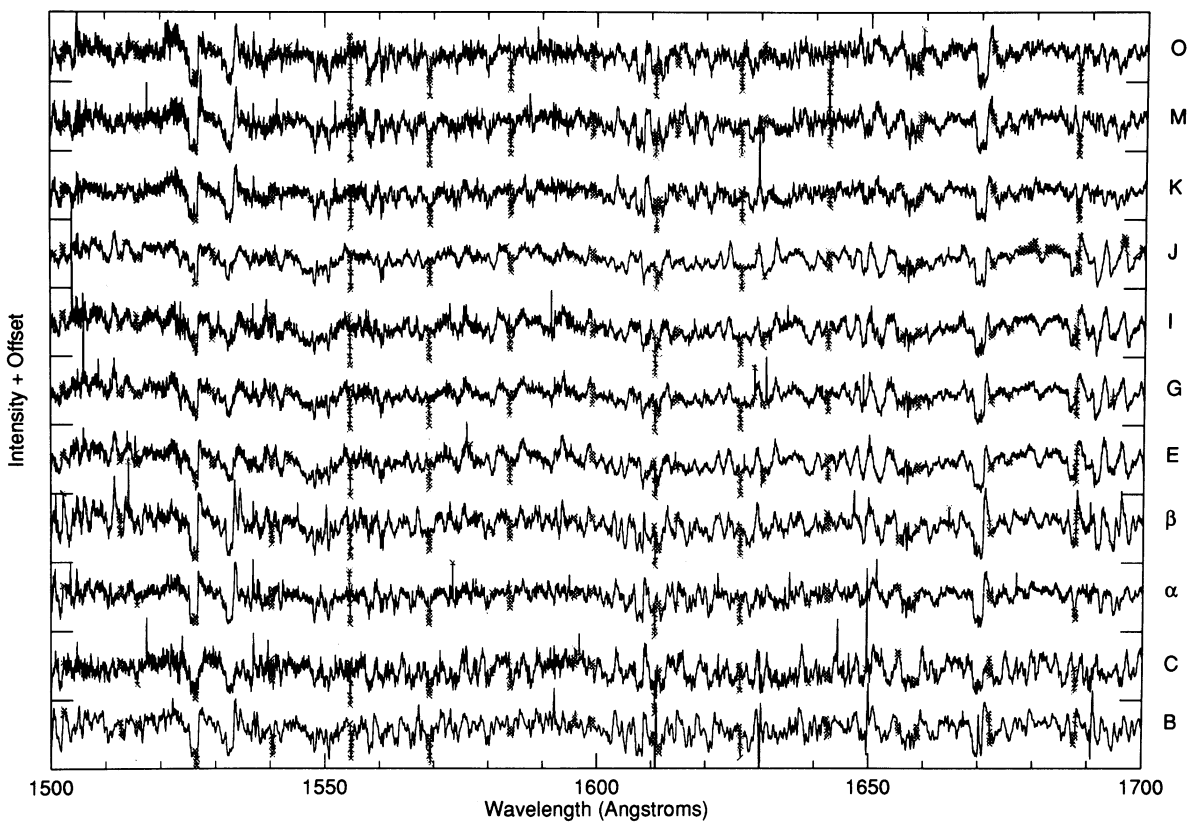

FIG. 9*b*

FIG. 9.—Montage of selected *IUE* high-dispersion spectra covering the period 1980 to 1992. Labels on the right vertical axis correspond to the labels in Fig. 1. (*a*) Wavelength region 1300–1500 Å. (*b*) 1500–1700 Å. (*c*) 2500–2700 Å. (*d*) 2700–2900 Å.

© American Astronomical Society • Provided by the NASA Astrophysics Data System

1994ApJ...428..292L

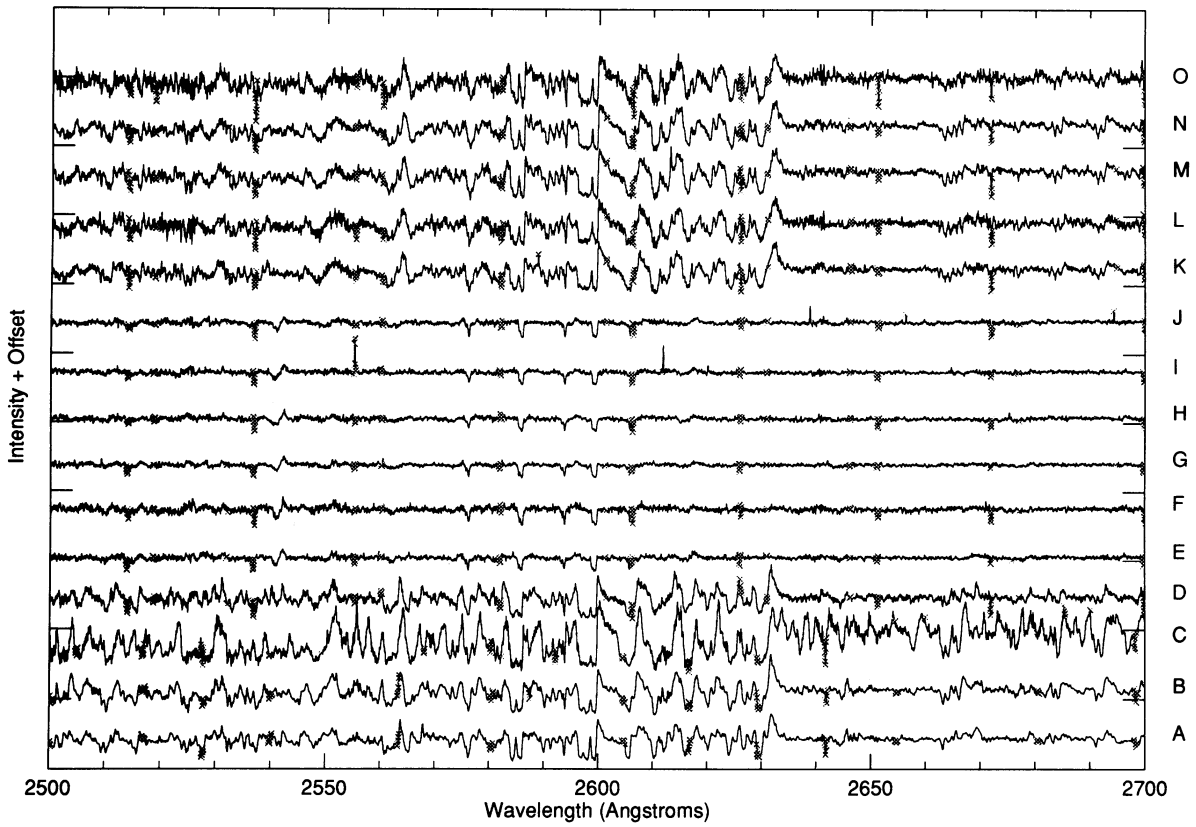

FIG. 9*c*

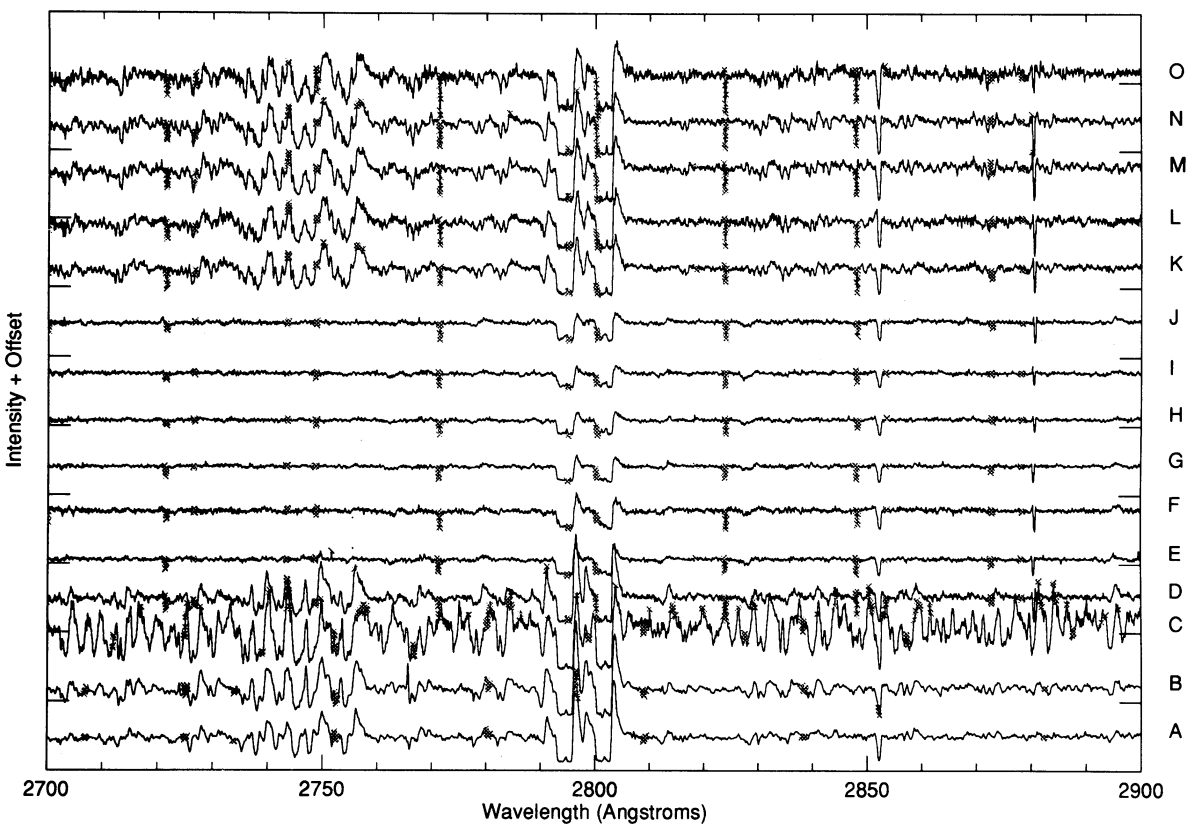

FIG. 9*d*

© American Astronomical Society • Provided by the NASA Astrophysics Data System

1994ApJ...428..292L

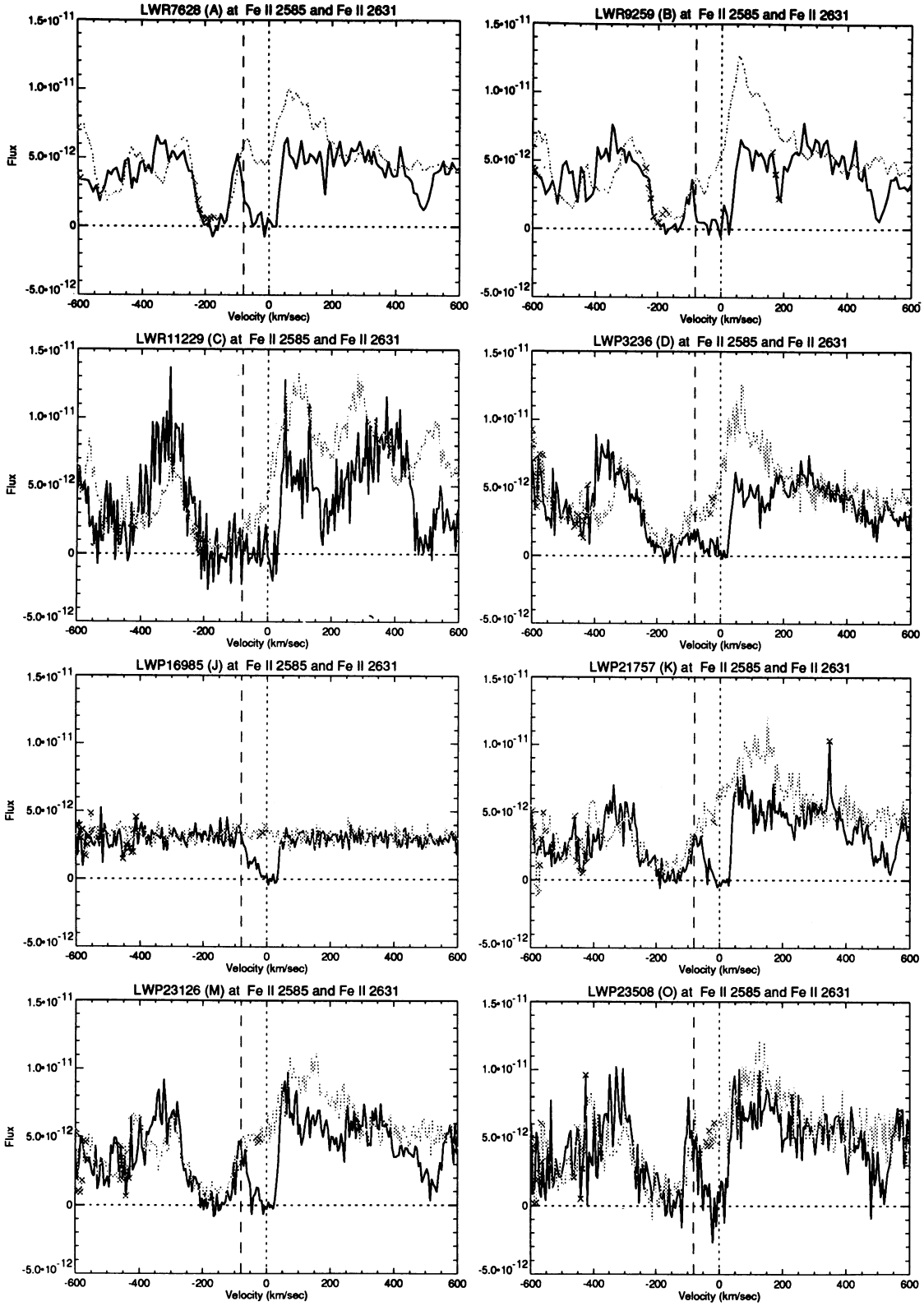

FIG. 10.—Selected profiles of Fe II λ2585 (*solid line*) and Fe II λ2631 (*dotted line*). Letters in parenthesis at the top of each figure refer to the epochs indicated in Fig. 1. Notice the different behavior of Fe II λ2585 (a resonance line) and Fe II λ2631 (an excited line). Vertical lines indicate the zero velocity, as well as the blue-edge velocity of the absorption feature at epoch J.

© American Astronomical Society • Provided by the NASA Astrophysics Data System

1994ApJ...428..292L

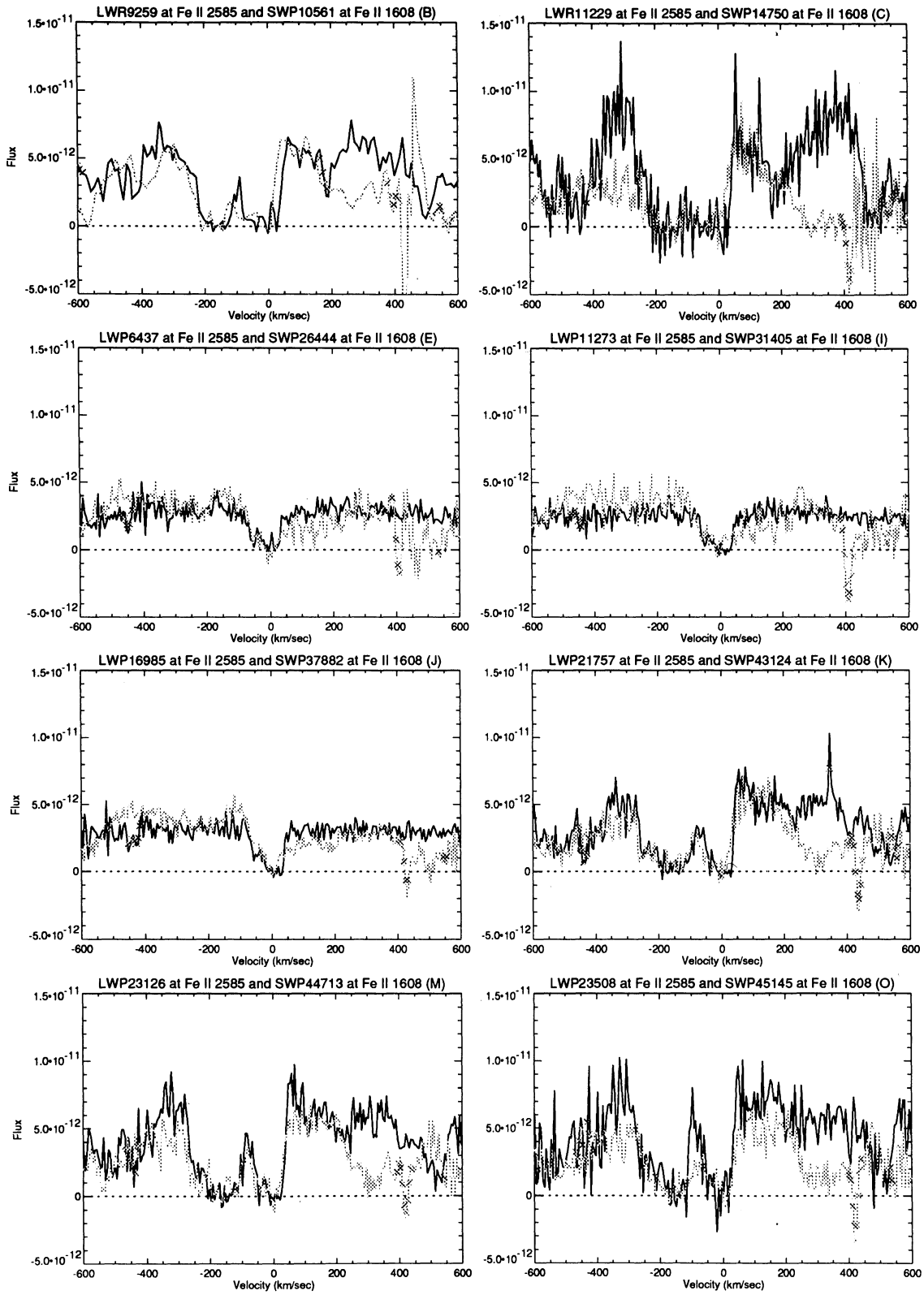

FIG. 11.—Same as Fig. 10, but for Fe II λ2585 (*solid line*) and Fe II λ1608 (*dotted line*). Both lines originate from ground states and have comparable oscillator strengths but were observed with different cameras.

© American Astronomical Society • Provided by the NASA Astrophysics Data System

1994ApJ...428..292L

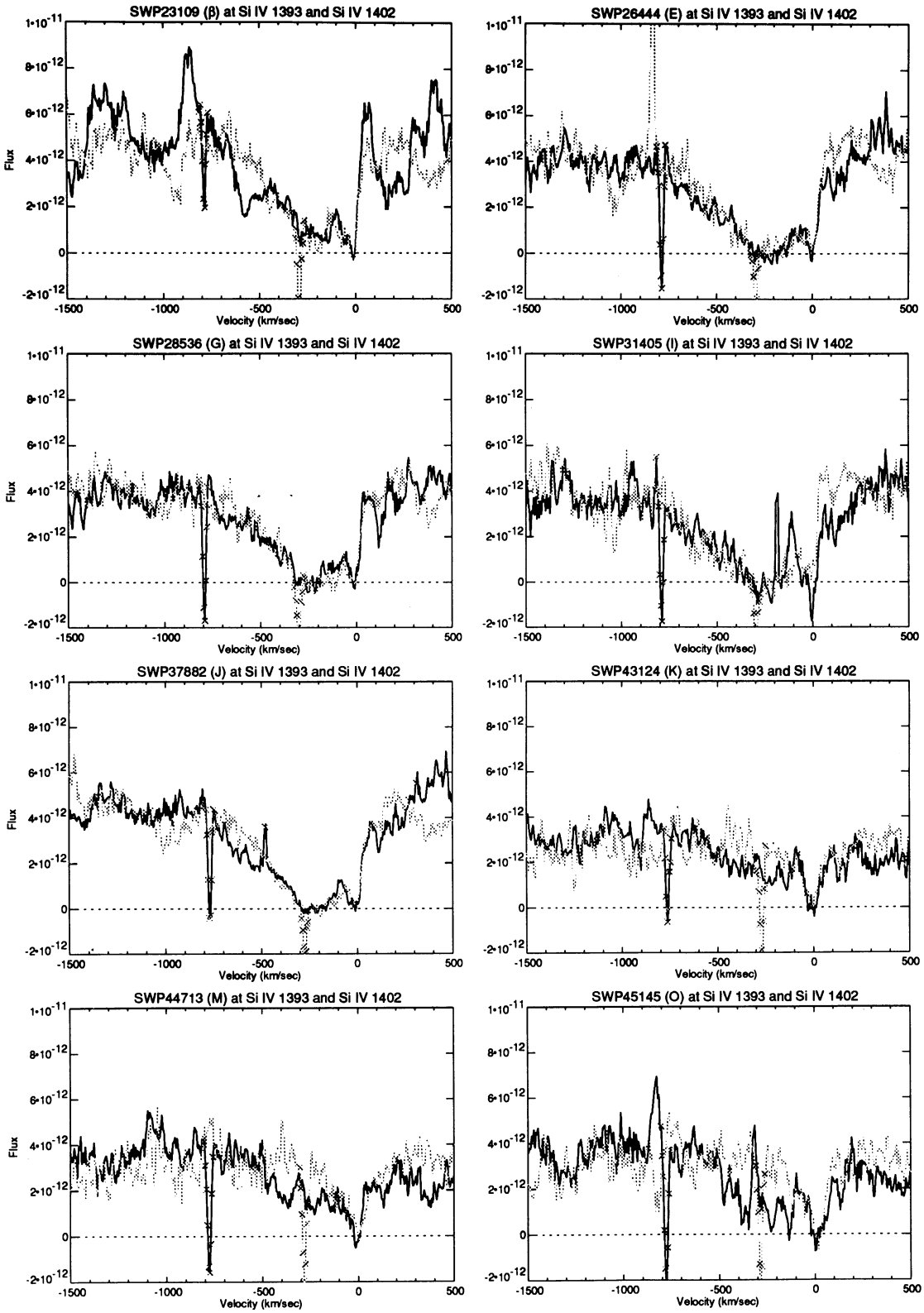

FIG. 12.—Same as Fig. 10, but for the Si IV doublet $\lambda\lambda$1393, 1402. *Solid line*: λ1393; *dotted line*: λ1402. The blue wings extend to velocities of up to -1000 km s^{-1}.

© American Astronomical Society • Provided by the NASA Astrophysics Data System

1994ApJ...428..292L

tion component in the OB supergiants. This fine structure may to some degree be due to contamination by photospheric Fe lines. Hubeny, Štefl, & Harmanec (1985) demonstrated that an iron blend at ~1400 Å can mimic the Si IV line in the photospheres of late-B stars. Therefore we cannot exclude the possibility that iron lines contribute to the absorption in the Si IV line, especially at epoch O (cf. Fig. 12).

Although wind velocities of up to 1000 km s^{-1} on the basis of Si IV are uncertain, the terminal velocities observed in the ultraviolet are definitely higher than in the optical, and they show hardly any variation. We find $v_\infty \approx 400$ km s^{-1} from the Fe II lines and possibly higher velocities from Si IV. This may be compared to the value seen in Hα, which does not exceed 250 km s^{-1} and may temporarily be as low as 50 km s^{-1} (cf. § 5). The coexistence of both a slow, dense wind and a faster, less dense wind is suggestive of the phenomena observed in Be and B[e] stars. We note that the velocity measured in the ultraviolet lines is high enough to make travel-time effects less important than in, e.g., the Hα line. Therefore the fast wind cannot be a relic of an earlier physical state of AG Car. Zickgraf et al. (1985) proposed a two-component wind for the B[e] star R126 based on its hybrid spectrum. On the one hand, narrow emission lines in R126 indicate the presence of a slow equatorial wind, and on the other, blueshifted ultraviolet absorptions suggest high wind velocities of 400 km s^{-1} or higher. Despite the somewhat lower terminal wind velocity observed in the lines of AG Car, the overall wind geometry of AG Car is very reminiscent of the situation in B[e] stars.

Curiously, in AG Car, the C IV doublet lines ($\lambda\lambda$1548, 1550) apparently do not participate in this high-speed flow, being rather narrow and only slightly asymmetric. Most likely this is an ionization effect, since the ionization potential of C III is more than 14 eV above that of Si III—unlike Si IV, the C IV lines show no dramatic change as AG Car varies in spectral type. Both Si IV and C IV, and even N V, provide important evidence of variable superionization in Be stars (see the review by Snow & Stalio 1987) and in B[e] stars (Zickgraf 1992). On the other hand, the C IV profiles in AG Car are consistent with a predominantly photospheric origin, supporting the view that Si IV might as well (at least partially) be contaminated by a photospheric contribution. This was also found to affect the determination of v_∞ in the Ofpe/WNL star R84 (Schmutz et al. 1991).

It is remarkable how constant the outflow velocity remained during the 12 years of *IUE* observations. No significant variation of v_∞ can be claimed on the basis of ultraviolet absorption lines. Most variations are due to changes in the wind- and stellar temperature which cause different ionization conditions. In contrast, the wind density and velocity *as observed in the ultraviolet* is relatively constant.

4.3. *Spectral Lines in the Optical*

In Figure 13 we show a selection of our ground-based spectra. The individual spectra in each figure are normalized to unity and displaced in the y-direction for clarity. The dates in the figure can be used to identify the spectrum in the log of observations in Table 5.

He I λ6678 exhibits a dramatic change from a strong emission and associated blueshifted absorption with a net equivalent width of 6.0 Å in 1990 December, to a very weak line with a net equivalent width of 1.7 Å in 1992 June. The behavior can be understood in terms of changing wind density and decreasing temperature. AG Car had an equivalent spectral type of late-O at the end of 1990 based on the presence of He II λ4686 (see Leitherer et al. 1992). Subsequently the He II feature faded, and we found no evidence for its presence in 1992 June. At that epoch the equivalent spectral type was approximately early- to mid-B. The equivalent width of He I λ6678 clearly correlates with the visual continuum flux, as can be seen in Figure 14. The values for the visual flux in this figure were derived from the data in Figure 1, after dereddening with $E(B-V) = 0.63$ and $A_V/E(B-V) = 3.1$. The value of $E(B-V)$ follows from our ultraviolet analysis under the assumption $L = \text{const}$. He I is strongest when the visual flux is highest. The visual flux rose continuously between 1990 December and 1991 December. During the first few months of 1992 the flux decreased but increased again after epoch 1992.3. Interestingly, He I shows exactly the same behavior. The errors of the equivalent width of He I (and also of Hα) are largely due to the uncertainties of the adopted continuum. Both He I λ6678 and Hα have broad, shallow line wings which contribute significantly to the total equivalent width. These wings are attributed to electron scattering in the outflow (see below). We estimate that the derived equivalent widths have errors of 10% or less. Therefore the rise of the He I equivalent width from 1991.9 to 1992.2 and the subsequent decline at 1992.4 is significant. It is also in accord with the observed profile change (cf. Fig. 13).

The decreasing temperature of AG Car during our observing period favored the appearance of spectral lines of lower ionization. Typical examples are the transitions at λ8629 and λ8680 of N I multiplets (8) and (1), respectively (see Fig. 13). These lines were absent in 1990 December when He II was still recognizable in the spectrum. They increased in strength at later epochs due to ionization conditions in the outflow which favored the formation of N°. At the same time, the profiles become narrower indicating a lower density and/or lower outflow velocity. The near-IR spectrum of AG Car resembles the one of η Car (Thackeray 1969) with respect to the presence of N I lines. This suggests rather similar temperature and density conditions in these two related objects. On the other hand, AG Car shows significantly stronger N I lines than P Cyg (see Stahl et al. 1993), although P Cyg is supposed to be related to LBVs (Humphreys 1989), and the spectral type of AG Car during 1991 was similar to the one of P Cyg (B1 Ia$^+$). This may suggest that nitrogen is more abundant in AG Car than in P Cyg but stronger observational support is certainly needed for this hypothesis.

Among the most striking characteristics of LBVs is the variability of ionized forbidden and allowed metal lines (e.g., Wolf 1989). The presence or absence of Fe II and [Fe II] lines can be used to describe the physical conditions in the stellar envelope (see Wolf, Appenzeller, & Stahl 1981 for R71). In Figure 13 we show the evolution of Fe II λ9997. This line has also been detected in η Car (Thackeray 1969) and is ascribed to the multiplet $z\,^4F^o_{9/2}$–$b\,^4G_{11/2}$ (Johansson 1977). Fe II λ9997 was first detected in 1991 August but is clearly absent in our spectra of 1990 June and December. Fe II λ9997 and the N I lines discussed before behave very similar in that respect. The similar ionization potential of Fe II (16.2 eV) and N I (14.5 eV) suggests that this is predominantly an ionization effect. Further support for this suggestion comes from the iron spectrum in the ultraviolet. The decrease in the strength of Fe II $\lambda\lambda$2585, 2599 during optical minimum, when AG Car was hottest, is most likely due to ionization from Fe$^+$ to Fe^{++} (see § 4.2). As in the case of the N I lines, we note the decreasing line width of Fe II λ9997 with time.

We observe both forbidden and allowed iron lines in the

© American Astronomical Society • Provided by the NASA Astrophysics Data System

1994ApJ...428..292L

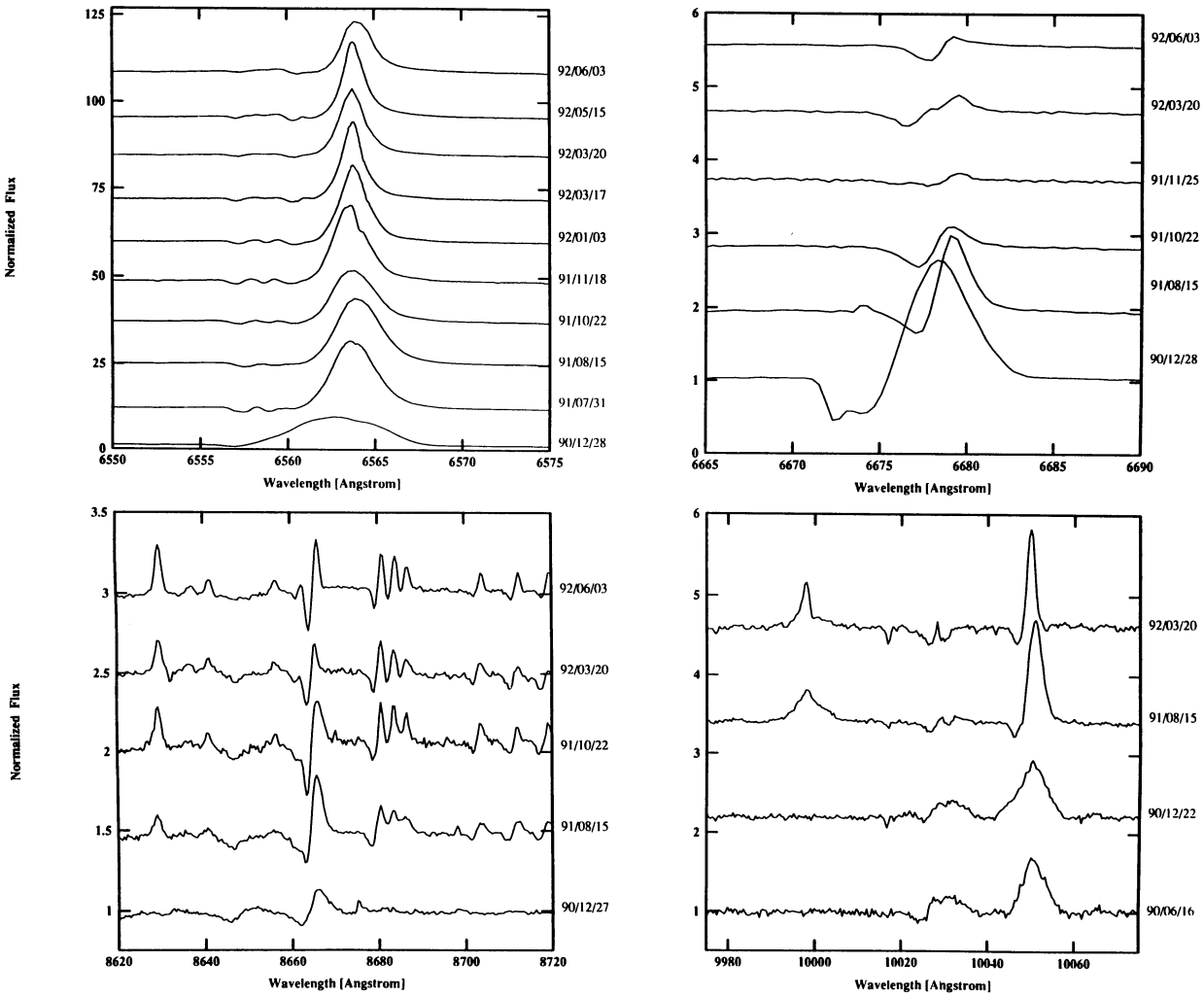

FIG. 13.—Ground-based spectra of AG Car. Four representative spectral regions are shown. The continua are normalized to unity and displaced by a constant δ in all cases. Spectral regions are around Hα (δ = 11.9), He I λ6678 (0.9), Fe II λ9997 (1.2), and N I multiplet (1) $\lambda\lambda$8680 (0.5). The sequence is clockwise, starting from upper left.

spectrum of 1992 June (Fig. 15). Wolf et al. (1981) and Leitherer et al. (1985) observed a correlation between the strength of these lines and the activity state of the LBV in R71 and S Dor, respectively. Forbidden lines dominate when the star is in its photometric minimum, i.e., hottest, and allowed lines take over during maximum state when the surface temperature is lowest. Comparison of Figure 15 with Figure 8 of Leitherer et al. (1985) suggests that the physical conditions in the envelopes of AG Car in 1992 June and of S Dor in 1984 August were somewhat similar. Close inspection of Figure 15 reveals that the profiles of Fe II and [Fe II] are quite different. Allowed lines [such as Fe II (27) λ4233 or Fe II (27) λ4352] are narrow. In contrast, forbidden lines {such as [Fe II] (21) λ4244 or [Fe II] (7) λ4287} are much broader and appear to be *flat topped*. [Fe II] λ4244 is generally formed at lower densities than Fe II λ4233 (Viotti 1976). Since flat-topped profiles are formed in an outflow with a constant velocity (Israelian & de Groot 1992), they could originate further out in the wind at lower densities where the terminal velocity of the outflow has been reached. The half-width of the lines suggest a velocity of $\sim$200 km s^{-1}. However, one should keep in mind that this does not indicate the terminal velocity of the material ejected from the stellar surface in 1992 June. Due to the flow timescale (several months), this value describes wind properties appropriate for an earlier epoch when the velocity was still higher (see below for a discussion).

Hα is the most prominent emission line in the observed spectrum during all epochs (see Fig. 13). Its main characteristics are: a strong emission component reaching up to 25 times the continuum level, broad, shallow electron scattering wings (these wings are not easily visible at the scale of Fig. 13), and several discrete absorption components. Hα is mainly a measure of the wind density, and to a smaller degree, of the stellar temperature. The variation of the equivalent width $W_{H\alpha}$ with time is plotted in Fig. 14. $W_{H\alpha}$ includes the emission part, the absorptions, and the broad wings. No attempt was made to remove the numerous telluric absorption lines in this wavelength region. Their effect on the Hα equivalent width is negligible. $W_{H\alpha}$ increased from the end of 1990 until mid 1991 and decreased again to its original level. The basic trend visible in Figure 14 remains unchanged if we exclude the broad wings from the measurement of $W_{H\alpha}$, although of course $W_{H\alpha}$ is then significantly decreased (by up to a factor of 2 after 1992 January). Figure 13 demonstrates that the variation of $W_{H\alpha}$ is

© American Astronomical Society • Provided by the NASA Astrophysics Data System

1994ApJ...428..292L

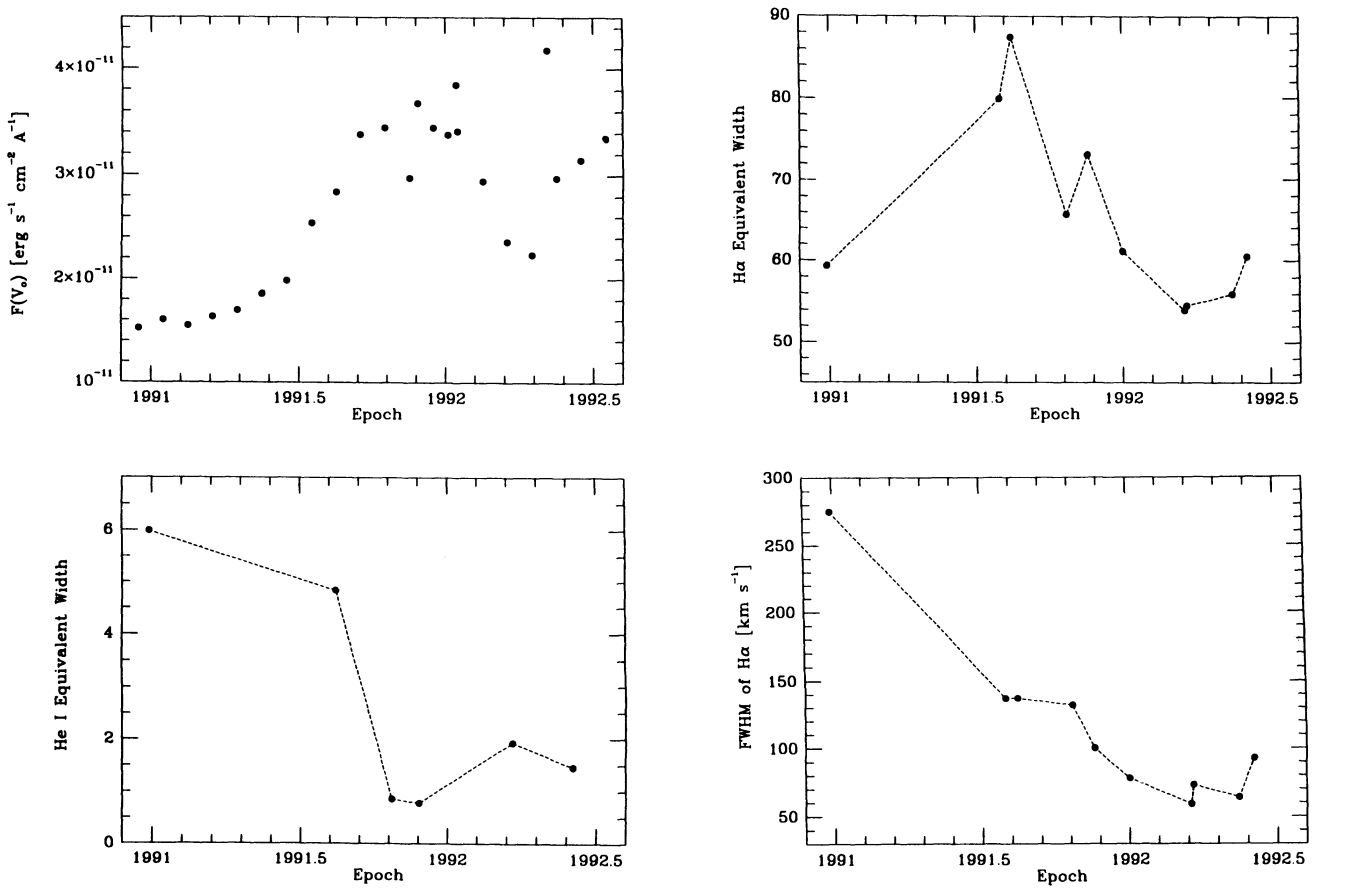

FIG. 14.—Variation of the dereddened continuum flux derived from visual observations, the equivalent widths of Hα and He I λ6678 (in angstroms), and the full width at half-maximum of Hα.

not simply due to a scaling of the line flux but that qualitative changes of the Hα profile occur. Hα is very broad in 1990 December. Subsequently, an increasingly pronounced emission core develops, which is narrowest between 1992 March and May. In 1992 June, the profile becomes broader again, resembling the situation in 1991 August. We measured the full width at half-maximum of Hα. The results are in Figure 14. The line width is determined by the outflow velocity. The decrease of FWHM suggests that the velocity decreased by about a factor of 4 during the observing campaign.

Other lines of hydrogen show the same qualitative behavior as Hα. We present P_7 λ10049 and P_{13} λ8665 as examples in Figure 13. P_{13} forms sufficiently close to the stellar surface that P Cygni absorption is visible during all epochs. The heliocentric velocity of the absorption component is -130 km s^{-1} in 1990 December and decreases to -50 km s^{-1} in 1992 March. This effect is also measured in the other Paschen lines. We do not expect the Paschen lines to indicate the terminal velocity of the outflow. Most likely, they form in the inner, still accelerating part of the wind. Interestingly, the velocity of the P_7 absorption component varied by a similar factor as the FWHM of Hα during the observing campaign. This suggests that the general shape of the velocity law is preserved although the flow velocity changed with time.

The variability of the outflow velocity detected in the hydrogen lines is very different from what is observed in the ultraviolet. Part of the difference may be due to travel-time effects. Hydrogen lines form closer to the star than typical strong ultraviolet resonance lines, and it will take a longer time to observe variations in the ultraviolet. However, the relative lack of variability *over 12 years of IUE* observations rules out this possibility as the only explanation. More likely, the wind conditions observed in the optical and the ultraviolet are really different. The optical wind spectrum is dominated by recombination lines which form in the densest part of the outflow,

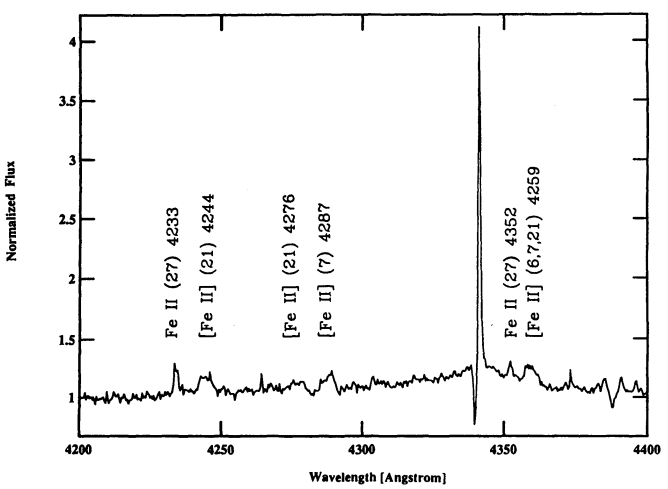

FIG. 15.—Spectrum of AG Car around 4300 Å at epoch 1992 June 3. Broad, flat-topped lines of [Fe II] and narrow lines of Fe II are present.

© American Astronomical Society • Provided by the NASA Astrophysics Data System

1994ApJ...428..292L

which in our proposed model is in the disklike equatorial density enhancement. The hydrogen and helium lines indicate that this is the most variable part of AG Car's wind. It is this part of the wind which is responsible for the observed polarization variation. In contrast, the high-speed outflow observed in the ultraviolet lines is rather constant and less affected by varying photospheric conditions.

It is instructive to compare the spectral morphology of the three related objects AG Car, P Cyg, and η Car. In Figure 16 we present the spectral region $\sim$10,000 Å of these three objects. The spectrum of AG Car is the one obtained in 1991 August shown in Figure 13. The spectra of P Cyg and η Car were taken with the same instrumentation at the Brazilian National Observatory in 1991. We discussed before the strength of the nitrogen lines in AG Car, which may suggest that the abundance of nitrogen in AG Car is closer to η Car than to P Cyg. However, Figure 16 demonstrates that the wind characteristics are clearly more pronounced in η Car than in AG Car. P_7 and Fe II λ9997 are by far stronger in emission in η Car than in AG Car. The emission-line spectrum of P Cyg is somewhat less extreme than the one of AG Car. Note the broader, P_7 emission of P Cyg. Also, the absorption component has a more negative blueshift in P Cyg than in AG Car. The maximum outflow of P Cyg is 200 km s^{-1} (Lamers, Korevaar, & Cassatella 1985). Therefore the comparison of the P_7 profiles suggests that the outflow velocity of AG Car in 1991 August was significantly less than 200 km s^{-1}. This is consistent with the result of our wind analysis (see § 5).

Figure 17 is a close-up of Figure 13 showing the absorption components shortward of Hα. We selected only those spectrograms having comparable spectral resolution of $\sim$0.1 Å. Four discrete absorption components are present. We find no significant radial velocity variation with time. The four components are at -250 km s^{-1}, -180 km s^{-1}, -110 km s^{-1}, and -70 km s^{-1} (heliocentric). The four components are highly variable in strength. In general, the faster components are stronger at earlier epochs, and the slower components become stronger during later times. The constant velocity of the absorption components suggests that they are formed in regions expanding at constant velocity, and the decreasing strength is simply a consequence of the decreasing density. An alternative explanation has been suggested by Hillier (1992). He demonstrated that multiple absorption profiles can as well be obtained purely from radiative transfer effects without the need of discrete shells.

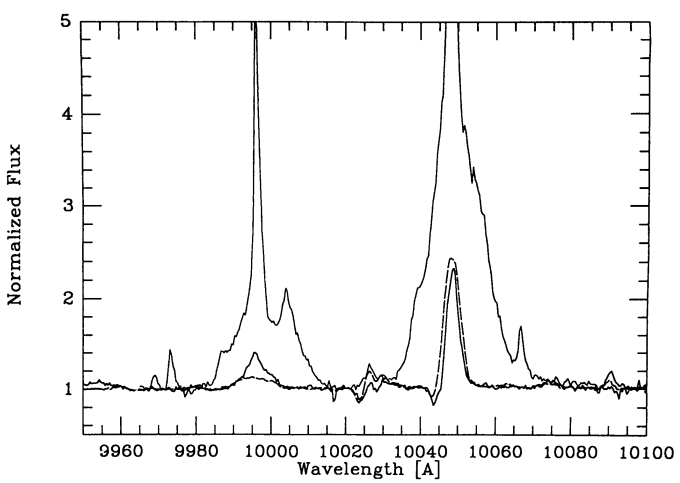

FIG. 16.—Comparison of the spectral region around P_7 in AG Car (*solid curve*), η Car (*dotted curve*), and P Cyg (*dashed curve*). The spectrum of AG Car was taken on 1991 August 15.

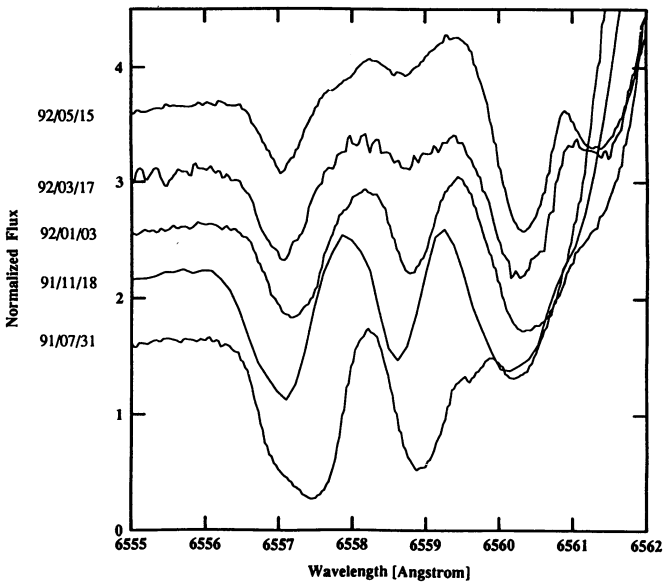

FIG. 17.—Blueshifted absorption components of Hα. All spectra plotted have similar spectral resolution of $\sim$0.1 Å. Spectra are normalized to unity. Offsets of 0.5 have been added.

5. STELLAR-WIND PROPERTIES DERIVED FROM EMISSION-LINE DIAGNOSTICS

5.1. *Method*

Theoretical models for the atmosphere of AG Car were computed with a code described by Hamann & Schmutz (1987). The radiation transfer is solved in the comoving frame, and the coupling between the transfer and the statistical equilibrium equations is treated with the approximate lambda iteration technique (Hamann 1987). The model atmosphere is expanding and spherically extended, as required by the physical conditions in LBVs. The radius of the photosphere is defined as the location where Rosseland optical depth unity is reached. The outflow velocity may be sub- or supersonic at this location. Strong photospheric absorption lines are virtually absent in the spectrum of AG Car so that the velocity of the photosphere is difficult to determine. Moreover, most lines which have their origin close to the photosphere are situated in the blue spectral region. This region is not well represented in our observational material. Wolf & Stahl (1982) studied the radial velocities of various lines in the AG Car spectrum. They found -26 km s^{-1} for Mg II λ4481. This line forms close to the location of the photosphere (cf. S Dor; Leitherer et al. 1985) and provides an upper limit to the velocity of the photosphere. The small expansion velocity of Mg II λ4481 is consistent with our models which predict negligible photospheric velocities. Optical depth unity occurs at a velocity of $\sim$10 km s^{-1} in all our models.

Leitherer et al. (1992) published line profiles obtained with the model atmosphere described above. An important improvement over the models shown in that paper has been made: we are now including electron scattering as an additional mechanism to reproduce the broad wings around strong

© American Astronomical Society • Provided by the NASA Astrophysics Data System

1994ApJ...428..292L

emission lines. Such wings are typically found in very luminous hot stars. Bernat & Lambert (1978) attributed these wings to electron scattering of line photons in the ionized stellar wind of P Cyg. In our present study, we do not attempt to perform a detailed profile fit of every hydrogen and helium line for each epoch. Rather, we calculated a grid of representative model atmospheres covering the parameter space occupied by AG Car. The equivalent widths of Hα ($W_{H\alpha}$) and He I λ6678 ($W_{He\,I}$) as well as the continuum flux at 5555 Å (F_{5555}) are predicted by each model. This approach is very similar to the one taken by Schmutz, Hamann, & Wessolowski (1989), who presented diagnostic diagrams for the derivation of mass-loss rates of Wolf-Rayet stars from their emission-line strengths.

The main reason for our simplified approach is that the nature of AG Car precludes a very detailed analysis with our models. We demonstrated in §§ 3 and 4 that significant asymmetries prevail in the circumstellar envelope. In contrast, spherical symmetry is assumed in the model atmosphere. The variability of AG Car introduces a further complication. The typical flow timescale (e.g., for a gas element to travel from the photosphere to 10 stellar radii) is several months. This is comparable to, or even longer, than the timescale over which significant continuum variability occurs. A time-independent model atmosphere cannot predict the line cores (formed at low velocities) and the line wings (formed at high velocities) at the same time. Therefore we expect *absolute* wind properties (such as the mass-loss rate) to be relatively uncertain. Our main goal, however, is to search for relationships between photospheric and wind parameters during the variability cycle, such as the *relative* change of the mass-loss rate. At least to first order, relative quantities are less affected by asymmetries and variability of the outflow.

5.2. *Results*

We assume $\log L/L_\odot = 6.0$ for the analysis. This is consistent with our analysis of the *IUE* data. A model is completely determined by the temperature $T_\star$, the transformed radius R_t, and the abundances of hydrogen and helium. $T_\star$ is the temperature at Rosseland optical depth unity. We used the observed flux at 5555 Å to constrain $T_\star$. F_{5555} is primarily sensitive to $T_\star$ and has only a comparatively weak dependence on the wind density. The parameter R_t has been defined by Schmutz, Hamann, & Wessolowski (1989). Essentially it is a measure of the inverse wind density and scales with the stellar radius $R_\star$ at $T_\star$, the mass-loss rate $\dot{M}$, and the wind velocity $v(r)$.

We adopt a velocity law of the form $v(r) = v_\infty(1 - R_\star/r)$ for the supersonic part of the outflow. This corresponds to the parameterization of the velocity law in hot stars (Groenewegen, Lamers, & Pauldrach 1989), but with a somewhat higher power-law exponent of 1. Support for this particular choice comes from profile fitting of selected emission lines of AG Car (Leitherer et al. 1992), which are well reproduced with this velocity law. The same velocity law was also derived by Schmutz et al. (1991) from a detailed multi-line analysis of the Ofpe/WNL star R84, which is believed to be in an evolutionary state closely related to LBVs (Hillier 1992).

This leaves the terminal velocity v_∞ as the only free parameter for the velocity law. As already discussed, the flow timescale of the wind is several months, whereas significant photospheric variations occur within a few weeks. Therefore emission-line wings (even after correction for electron scattering) or blueshifted absorption components are difficult to use to derive v_∞ at a particular epoch if rapid changes in the wind properties occur. These features respond to changes in the inner part of the outflow only after several months. On the other hand, the line core of Hα forms much closer to the stellar photosphere and has a much shorter response time to changes in the outflow velocity. We compared the FWHM of Hα to v_∞ at epochs when v_∞ could be reliably determined from profile fits. Leitherer et al. (1992) found $v_\infty = 250$ and 120 km s^{-1} at epochs 1990 December and 1991 August, respectively. The decrease of v_∞ by a factor of 2 is also reproduced by FWHM, which also decreases by a factor of 2 (cf. Fig. 14). We assumed that the same scaling holds for subsequent epochs and calculated v_∞ from the full width at half-maximum of Hα after calibration with the derived values of v_∞ at 1990 December and 1991 August. The results are in Table 9.

The decrease of the outflow velocity deduced from the FWHM of Hα is also supported by the variable Hα absorption components (see Fig. 17). The fastest component at −250 km s^{-1} gradually decreased in strength from 1991 July to 1992 May. During this period, slower components increased in strength. The slowest absorption component observed is at −70 km s^{-1}. The presence of discrete components suggests that mass loss does not occur steadily but rather in a discontinuous way. The increase in strength of low-velocity components and the fading of high-velocity components are in agreement with an overall decrease of v_∞ of the wind region where Hα is formed. (Note that travel-time effects must be taken into account when comparing v_∞ derived from the absorption components and from FWHM).

Our arguments relating to the velocity field of AG Car's wind are only applicable if the wind is spherically symmetric. However, the results of the spectropolarimetry and the ultraviolet spectroscopy indicate the presence of an equatorial density enhancement. We expect optical recombination lines of hydrogen and helium to form preferentially in this equatorial region. This is consistent with our approach not to use the ultraviolet lines for a determination of v_∞ but to rely exclusively on Hα. On the other hand, it is likely that the equatorial wind has nonzero angular momentum. Therefore the observed line width of Hα may not only be caused by the outflow velocity but may also be influenced by rotation. However, we estimate the rotational broadening of Hα to be small as compared to the broadening caused by the outflow velocity. A reasonable upper limit to the rotation of the disk material is the rotational velocity of the star itself. In the course of its evolution from the main sequence to the LBV phase, AG Car's radius increased by at least an order of magnitude. The star could not have been gravitationally bound on the main sequence due to the high

TABLE 9

PROPERTIES OF THE STELLAR WIND

Epoch	$T_\star$ (K)	$R_\star$ ($R_\odot$)	FWHM(Hα) (km s^{-1})	v_∞ (km s^{-1})	log $\dot{M}$(H) ($M_\odot$ yr^{-1})
1990 Dec	21,000	76	275	250	−4.7
1991 Jul	16,000	120	137	120	−4.4
1991 Aug	16,000	130	137	120	−4.6
1991 Oct	14,000	160	132	120	−4.7
1991 Nov	14,000	160	100	90	−4.8
1992 Jan	14,000	160	78	70	−5.0
1992 Mar	17,000	110	59	50	−5.2
1992 May	15,000	140	64	60	−5.1
1992 Jun	15,000	150	93	80	−4.9

© American Astronomical Society • Provided by the NASA Astrophysics Data System

1994ApJ...428..292L

rotational velocity if a solid rotator model is assumed and if the present rotational velocity exceeded of few tens of km s^{-1}.

The grid of model atmosphere was calculated with equal abundances (*by mass*) for hydrogen and helium, i.e., $X = Y = 0.5$. In principle, the helium abundance of a hot star can be determined from an analysis of the type presented here once the mass-loss rate and the stellar temperature are constrained (see, e.g., Schmutz et al. 1991). In the case of AG Car $\dot{M}$ can be derived almost independently either from the hydrogen or the helium lines. However, the neutral helium lines are sensitive to both the temperature and the helium abundance. Without simultaneous modeling of He II lines, the temperature cannot be constrained (e.g., from F_{5555}) precisely enough to allow a reliable abundance analysis.

The results of our atmospheric analysis of AG Car are summarized in Table 9. $T_\star$ and $R_\star$ were first determined from the visual continuum flux, after normalization to the total bolometric luminosity. Subsequently, we verified that the choice of $T_\star$ reproduces the observed strength of He I λ6678 after the wind density was known from fitting the observed Hα strength. We find that $T_\star$ decreases from 21,000 to 15,000 K between 1990 December and 1992 June. Note that the slightly lower temperatures than in Leitherer et al. (1992) are a consequence of the smaller luminosity adopted here ($10^{6.0}$ vs. $10^{6.2}$). At the same time, the stellar radius increased by a factor of 2. This of course is a consequence of the assumption L = constant. We also derived the $T_{\rm eff}$ and $R_\star$ by fitting a classical Kurucz (1979) model atmosphere to the continuum. The results are not significantly different from those of the non-LTE analysis.

In Table 9 we list the mass fraction lost in hydrogen only. As helium makes a significant contribution to the total mass loss (see below), the values of $\dot{M}(H)$ are a lower limit to the total mass-loss rate. Despite the significant variation of the photospheric parameters, the mass-loss rate did not increase. Leitherer et al. (1992) already found that $\dot{M}$ of AG Car does not vary significantly with phase. We confirm their result and extend it to an even wider range of photospheric parameters. Contrary to previous suggestions (Lamers 1987), $\dot{M}$ does *not* scale inversely with temperature. The mass-loss rate is not higher when AG Car is cooler and visually brighter. In fact, if there is a correlation in the data of Table 9, it is just in the opposite sense: $\dot{M}$ is *lower* at the beginning of 1992 than in 1990 December although the temperature had dropped by 6000 K. However, the decrease in $\dot{M}$ is mostly due to the lower v_∞. Recall that we adopted v_∞ as derived from Hα, which displayed significant variability. On the other hand, the ultraviolet lines do not indicate any significant variation of v_∞ between the epochs of our observations. We argued above that Hα and the ultraviolet lines originate in different wind regions. Our non-LTE analysis refers to those parts of the wind where optical recombination radiation originates, which most likely is in the disklike equatorial density enhancement. The ultraviolet lines are unlikely to indicate the terminal wind velocity in this region. If this is not true, v_∞ used in our non-LTE analysis after 1990 December would be too low, and the derived $\dot{M}$ would be too low, too. Therefore, we do not claim that $\dot{M}$ actually *decreased*. But even under the very conservative assumption of v_∞ = *constant* during all epochs, $\dot{M}$ would at least *not increase* for lower temperatures.

We estimated the He abundance of AG Car from the spectroscopic data of 1990 December. At that epoch AG Car had the highest temperature, and the theoretical models are least sensitive to temperature variations. The mass-loss rate in helium is log $\dot{M}$(He) = -4.1. This suggests that the total mass rate including both hydrogen and helium is $10^{-4.0}\ M_\odot\ {\rm yr}^{-1}$. The helium abundance is $Y \approx 0.8 \pm 0.1$. This value has a relatively large error but taken at face value it suggests that the total mass-loss rate of AG Car can be derived by increasing the entries for $\dot{M}(H)$ in Table 9 by 0.7 dex. The average total (H + He) mass-loss rate during our observational campaign is $\dot{M} = 10^{-4.1}\ M_\odot\ {\rm yr}^{-1}$. We emphasize the uncertainties associated with this value: the uncertain helium abundance, the velocity law, the variability of the outflow, and deviations from spherical symmetry. However, the main new result is the constancy (or probably even decrease) of $\dot{M}$, and this result is much less affected by such uncertainties.

6. AG CARINAE: LBV ROSETTA?

6.1. *Relation between the Photosphere and $\dot{M}$*

The nearly constant (or even decreasing) mass-loss rate of AG Car over a period when the effective temperature decreased significantly is surprising and in disagreement with what was previously thought to be a general property of LBVs (see Lamers 1989). Historically, the first (so far the only) LBV for which an anticorrelation between $\dot{M}$ and $T_{\rm eff}$ could be established was R71. Wolf et al. (1981) found that the mass-loss rate of the S Dor variable R71 varied by one to two orders of magnitude between minimum and maximum state. Leitherer, Abbott, & Schmutz (1989) subsequently demonstrated that such behavior can be understood if radiation pressure drives the optically thin wind and if a subatmospheric mechanism can be identified to increase to stellar radius. The similarity of the spectral morphology suggests that the same arguments apply to the prototype of the S Dor variables, S Dor (=R88) itself (Leitherer et al. 1989). Although it has become customary to extend these results, which were obtained for an LBV subclass, to other LBVs as well, our present study shows that this generalization is invalid. AG Car does not exhibit the $\dot{M}$ versus $T_{\rm eff}$ relation observed in R71 and S Dor (at least not in the temperature range covered in this study).

What can be said about other LBV's? Little observational material exists which would allow us to prove or reject a correlation between mass loss and temperature in other LBVs. Leitherer et al. (1992) suggested that the LBV R127 behaves in a way very similar to AG Car. Comparison of the optical spectrum of R127 when it was hottest (late O; Stahl et al. 1983) and coolest (early-A; Wolf 1992) supports the view that no significant mass-loss variation occurred between these spectral phases. On the other hand, R110 did show temperature-dependent mass-loss variations but in just the opposite sense: $\dot{M}$ was lower at lower temperature (Stahl et al. 1990). Leitherer & Langer (1991) interpreted the lower mass-loss rate as a property of a radiatively driven wind. The stellar radiative momentum flux in the ultraviolet decreases dramatically if $T_{\rm eff} < 8000$ K and the kinematic momentum flux of the outflow is correspondingly low. The lower mass-loss rate is therefore a natural consequence of a radiatively driven wind if the effective temperature becomes lower. The problem still remains which mechanism is capable in modifying the photospheric temperature. Recently Sterken et al. (1991) discovered the galactic star HD 160529 as a new addition to the LBV family. An analysis of the mass loss during several epochs when HD 160529 varied between spectral types early-A and late-B resulted in $\dot{M} \approx$ const.

We conclude that *there is no observational support for a*

© American Astronomical Society • Provided by the NASA Astrophysics Data System

1994ApJ...428..292L

unique relation between photospheric temperature (or radius) and mass-loss rate among LBVs. Some LBVs have higher mass-loss rates at lower temperature, at least one shows the opposite behavior, and in some LBVs (including AG Car) the temperature variations occur at approximately constant mass-loss rate. Such behavior was also suspected by Wolf (1992). AG Car and HD 160529 have vastly different stellar parameters: AG Car is among the most luminous and hottest LBVs, whereas HD 160529 is one of the least luminous ($L \approx 4 \times 10^5\ L_\odot$; Sterken et al. 1991) and coolest ($T_{\rm eff} = 8000$ K; Sterken et al. 1991). Yet both show the same behavior with respect to the mass-loss rate.

The lack of correlation between photospheric radius and temperature on the one hand, and $\dot{M}$ and the other is incompatible with a model which ascribes the radius variability to optical depth variations in a wind with variable mass-loss rate. This has been suggested by Appenzeller (1986) and Davidson (1987). In principle, such a model could account in a self-consistent way for the observed radius and mass-loss variability in objects like R71 and S Dor. However, Leitherer et al. (1989b) and de Koter (1993) computed radiative wind models to investigate the proposed radius increase with increasing mass-loss rate in a quantitative way. It was found that optical depth effects alone cannot explain the radius variability in R71 and S Dor and that the mechanism responsible for the variable photospheric parameters still needs to be identified. AG Car provides additional observational proof for this theoretical result. $T_{\rm eff}$ and $R_\star$ vary without a significant variation of $\dot{M}$.

6.2. *Geometry of the Stellar Wind*

Traditionally, spherical symmetry has often been assumed for the geometry of the outflows from LBVs. The results from our spectropolarimetry indicate that deviations from spherical symmetry exist in AG Car. Is AG Car unique in this respect, or do related objects show similar evidence for asymmetries in their winds?

The small level of intrinsic, variable polarization found in some O supergiants (Lupie & Nordsieck 1987 and references therein) has been attributed to density perturbations in the wind, also observed as discrete absorption components in the UV spectra of O stars. The high and variable intrinsic polarization observed in Be and B[e] stars ($\sim$1%–2%; Poeckert, Bastien, & Landstreet 1979; Zickgraf & Schulte-Ladbeck 1989) is thought to originate from the high-density contrast between the equatorial and polar winds (Cassinelli et al. 1987). Extensive broad-band polarization monitoring of single Wolf-Rayet stars (Drissen et al. 1987; Robert et al. 1989) has shown that the wind structure of most Wolf-Rayet stars is variable ($\Delta P \approx 0.1\%$–0.6%) on timescales of hours to days. As in the case of OB stars, these variations are attributed to condensations of material being randomly ejected from the star. Contrary to Be stars, the random distribution of the data points shows no indication of a global asymmetry in the wind structure for the vast majority of single Wolf-Rayet stars (although a few noticeable exceptions have been found by Schulte-Ladbeck, Meade, & Hillier 1992 based on spectropolarimetric data).

All LBVs observed so far show relatively high levels of intrinsic polarization, indicative of nonspherically symmetric outflows. The brightest and most spectacular Galactic LBV, η Car, is embedded in a very complex gas and dust shell resulting from last century's eruption (Davidson 1989). Hester et al. (1991) detected a jetlike feature pointing away from η Car. High-resolution spectroscopy by Meaburn et al. (1993) confirms that the object has the characteristics of a true interstellar jet. Although there is no observational proof so far that AG Car's resolved bipolar outflow also satisfies the definition of a true jet, a similar physical mechanism for the origin of the "jets" in η Car and AG Car seems plausible.

Imaging polarimetry (Warren-Smith et al. 1979) reveals very high levels of polarization (up to 35%) in the homunculus, in an almost centrosymmetric pattern. Such high levels are produced by scattering of the stellar light by dust particles. The dust is not spherically distributed and strongly attenuates the central object η Car (Hillier & Allen 1992). Because of the dense surrounding shell, very little is known about the polarization properties of the central star itself. The variation in the global polarization observed 20 yr apart (Gnedin et al. 1992) could have been caused by dust redistribution in the shell.

P Cygni shows intrinsic and variable polarization (up to 0.6%; Hayes 1985; Taylor et al. 1991). The absence of a persistent topology in the distribution of the data points in the $Q-U$ diagram of P Cyg argues in favor of ejection of clumps or plumes in random directions rather than in a preferred plane. This agrees rather well with the results of other, independent techniques. White & Becker (1982) resolved P Cyg's stellar wind by radio interferometry and found that the visibility function is consistent with a spherically symmetric wind. Clampin (private communication) obtained coronographic images of the nebulosity detected by Leitherer & Zickgraf (1987) and Johnson et al. (1992). The nebulosity is characterized by a remarkable degree of symmetry.

Large polarization variation across the Hα emission line has been observed in the LMC LBV R127 (Schulte-Ladbeck et al. 1993). The intrinsic polarization of this star (1%–1.5%) is much higher than that of P Cyg, and a global distortion of the wind, similar to that of Be stars, is favored in this case. Clampin et al. (1993) found clear evidence for axial symmetry in the resolved nebula around R127—in contrast to P Cyg which was observed with the same observational technique. Further support for stronger deviations from spherical symmetry in R127's wind (as compared to P Cyg) comes from the detection of inverse P Cygni profiles in R127. Schulte-Ladbeck et al. (1993) suggested a disklike geometry to explain the occasional presence of *redshifted* absorption lines.

How does AG Car compare with these objects? AG Car's intrinsic level of polarization is at least 0.5%. This value is much higher than the vast majority of normal OB and Wolf-Rayet stars. It compares well with that of P Cyg, but on the other hand is not as high as the intrinsic polarization observed in Be stars and the LBV R127.

The most striking observation comes from the fact that the polarization was relatively high in the 1991 November data, went down to an almost negligible value in 1992 May, and *came back up to almost identical values, both in amplitude and position angle* 2 months later, in 1992 July. This behavior suggests that the wind's asymmetry that gave rise to the high polarization had almost identical geometrical configurations in November and July, and vanished in May. Schulte-Ladbeck (private communication) also observed a very low value of optical continuum polarization in 1992 March.

Although the lack of continuous monitoring in the UV prevents us from developing a unique model for AG Car, it is tempting to suggest a model—proposed before for related stars—that is at least consistent with the few observations we have. The "preferred plane" observed in our UV data could be

© American Astronomical Society • Provided by the NASA Astrophysics Data System

1994ApJ...428..292L

interpreted as resulting from a rotationally induced density contrast between the equatorial wind of AG Car and its polar counterpart. Our data do not favor the presence of a thick disk around AG Car (since the intrinsic polarization is not extremely high), but Taylor & Cassinelli (1992) have shown that even a relatively low density contrast (factor of 2) between the equatorial and polar winds of massive stars could produce wavelength-dependent polarization of $\sim 1\%$. The presence of a global asymmetry in the wind is also supported by Schulte-Ladbeck (private communication), who observed large variations of both P and θ across the Hα emission line of AG Car.

It is interesting in this context to note that there are indications that the mass-loss rate was lower between March and May (Table 9) and increased again later on. This drop in the mass-loss rate could have resulted in a lower contrast between the equatorial and polar winds, reducing the amount of intrinsic polarization. We carefully note, however, that although this interpretation is consistent with the observations, it is by no means unique, and in particular the possible correlation between the mass-loss rate and polarization needs to be verified.

Although the geometry derived from the polarization data may not be entirely convincing by itself, it receives further support from the *IUE* results. The hybrid spectrum—lower wind velocities in optical emission lines and higher velocities in ultraviolet absorption lines—is naturally explained by a two-component wind with a relatively fast polar outflow and an equatorial density enhancement leading to a slower, dense wind. This is strikingly similar to the geometry found in the outflows from B[e] stars. Therefore the wind properties of LBVs and B[e] stars may be more similar than previously thought. This similarity provokes the suggestion that there may also be an evolutionary relation between LBVs and B[e] stars.

6.3. *Evolutionary Status of AG Carinae*

We compared the observed position of AG Car in the Hertzsprung-Russell diagram to model predictions by Schaller et al. (1992). The high helium abundance found in the non-LTE analysis implies that a large fraction of the original hydrogen-rich surface layer has already been lost. In fact, $Y \approx 0.8$ is predicted only by models with initial masses greater than 40 $M_\odot$ evolving from red to blue toward the Wolf-Rayet phase. A star with an initial mass of $M_i = (50 \pm 10)\ M_\odot$ at the entrance of the Wolf-Rayet phase is consistent with the derived luminosity, effective temperature, and helium abundance. The current mass would then be $(30 \pm 10)\ M_\odot$. The derived value of M_i leaves open the question if AG Car is currently in a post–red supergiant phase. Due to the uncertainties in the evolutionary models and in the value of M_i itself we cannot exclude the possibility that AG Car went through the red supergiant phase.

Schaller et al's models predict a nitrogen overabundance at the stellar surface of a factor of 16 with respect to the zero-age main sequence. Conversely, carbon and oxygen should be strongly deficient. We already noted the strength of neutral nitrogen lines in AG Car compared to P Cyg. In principle, the nebula surrounding AG Car should provide the clue for the presence or absence of a nitrogen overabundance. Mitra & Dufour (1990) measured a very high N/S ratio but rejected a nitrogen overabundance in favor of a sulfur underabundance. Their result—if indicative of the nitrogen surface abundance of AG Car—would be entirely incompatible with the proposed evolutionary state of AG Car. Nota et al. (1992) argued that the nebula could have been ejected during an earlier epoch when AG Car had not yet developed CNO anomalies at the surface. This hypothesis would be consistent with evolutionary calculations and the dynamical timescale of the nebula. De Freitas Pacheco et al. (1992) reanalyzed the chemical composition of the AG Car nebula and favor a nitrogen overabundance by an order of magnitude. Their result would be consistent with the stellar parameters derived here, under the assumption the composition of the nebula reflects the surface composition of AG Car. In view of the importance of the nitrogen abundance in AG Car, more work is urgently needed to settle the question of the chemical composition of the nebula.

We find that AG Car has parameters very close to WNL stars. The chose connection between AG Car (and the related object He 3-519) has recently been emphasized by Smith, Crowther, & Prinja (1994) on the basis of similar spectral morphology. These authors suggested to assign a new spectral class of WN 11 to AG Car. According to Smith et al. there may be a deeper astrophysical connection: AG Car could be considered as a Wolf-Rayet star making an excursion into the variability strip of the Hertzsprung-Russell diagram occupied by LBVs, rather than a LBV entering the Wolf-Rayet phase.

7. CONCLUSIONS

Is AG Car the Rosetta Stone for the LBV phenomenon? Due to its brightness, it is the LBV with the highest-quality observational material available. Two key results were found as a consequence of our observing campaign and theoretical modeling of AG Car: (1) *The stellar wind geometry deviates from spherical symmetry and has a two-component structure.* (2) *There is no indication for a positive correlation between stellar radius and mass-loss rate.*

We detected significant, variable intrinsic polarization in AG Car, which is interpreted as due to electron scattering, possibly modified by hydrogen and metal line absorption in a non-spherically symmetric stellar wind. Similar results have already been found for other luminous stars. Since a systematic study of the intrinsic polarization of LBVs has not yet been done, it cannot be excluded—and it appears plausible—that significant deviations from spherical symmetry are a general property of all LBVs. Further support for this generalization comes from the increasing number of detections of aspherical nebulosities around LBVs. η Car (Hester et al. 1991), AG Car (Nota et al. 1992), HR Car (Hutsemékers & Van Drom 1991a), WRA 751 (Hutsemékers & Van Drom 1991b), R127 (Clampin et al. 1993), and S119 (Nota et al. 1994) are now known to be surrounded by resolved nebular ejecta. High-resolution imaging reveals striking similarities in their morphology. In particular, axial symmetry with density enhancements in the equatorial plane is found in AG Car, R127, and S119. The geometry favored by us for inner wind region of AG Car is quite similar to the geometry of the distant, spatially resolved nebula. Therefore it is plausible that the morphology of the AG Car nebula is not a result of the interaction between AG Car's stellar wind and the ambient ISM, but is already determined by the physical conditions close to the stellar photosphere. However, we caution that the AG Car nebula is not a product of a stellar wind similar to the one presently observed. Rather, it was formed in a much more dramatic outburst $\sim 10^4$ yr ago.

Independent support for an equatorial density enhancement of the wind comes from the spectroscopic observations in the ultraviolet. We find evidence for a two-component wind. A

© American Astronomical Society • Provided by the NASA Astrophysics Data System

1994ApJ...428..292L

slow, dense wind observed in recombination lines and a less dense, faster wind observed in the absorption components of ultraviolet lines. The density enhancement in the equatorial plane of AG Car's stellar wind is reminiscent of the geometry suggested for the outflows from B[e] stars (Zickgraf 1992). Until now, there has been little evidence for a connection between LBVs and B[e] stars, except for the fact that they occupy roughly the same part of the Hertzsprung-Russell diagram. Shore (1992) noted some striking similarities in the ultraviolet spectra of LBVs and B[e] stars. Our results for AG Car hint at a closer connection than previously thought. Possibly the same mechanism is responsible for axial symmetry in the winds of LBVs and B[e] stars. Lamers & Pauldrach (1991) proposed an explanation for the existence of "disks" in B[e] by means of a bistability mechanism in radiatively driven winds. This mechanism may also have an application in the wind of AG Car.

One of the most striking properties of LBVs is the variability of photospheric and wind parameters. Incidentally, both the flow timescale of the optically thin wind and the dynamical timescale of the optically thick photosphere are comparable in AG Car (weeks to months). Therefore the timescales observed to occur in the outflow bear few clues for the origin of the variations. We find no evidence for an increasing mass-loss rate when AG Car's radius increased by a factor of 2. This result is new and has significant consequences for models attempting to explain the origin of the radius variability in LBVs in general. The radius variability in AG Car cannot be only due to opacity variations in the outflow, a result which has been suggested by us previously for R71 and S Dor (Leitherer et al. 1989b). However, our coverage of AG Car's activity cycle is still incomplete. If the light curve of AG Car can be extrapolated into the future, we expect a decrease of the effective temperature down to below 10,000 K in the next 2–3 years. It will be crucial to determine the wind properties in this temperature regime in order to assess if the relation between $\dot{M}$ and $R_\odot$ continues to hold. Intensive monitoring of AG Car in all accessible wavelength bands and observing modes holds the key for deciphering the Rosetta stone AG Car.

We gratefully acknowledge award of Director's Discretionary Time during which part of the *HST* observations were performed. Some spectroscopic observations at ESO were kindly performed by U. Mürset. M. McMaster assisted in the data reduction at STScI. A. Damineli acknowledges financial support by FAPESP. Support for this work was provided by NASA through grant number GO-3663.03-91A from the Space Telescope Science Institute, which is operated by the Associaton of Universities for Research in Astronomy, Inc., under NASA contract NAS 5-26555.

REFERENCES

Ake, T. B. 1981, NASA *IUE* Newsletter, 15, 60
———. 1982, NASA *IUE* Newsletter, 19, 37
Allen, R. G., & Angel, J. R. P. 1982, in Instrumentation in Astronomy IV, Proc. SPIE 331, 259
Allen, R. G., Smith, P. S., Angel, J. R. P., Miller, B. W., Anderson, S., & Margon, B. 1993, ApJ, 403, 610
Appenzeller, I. 1986, in IAU Symp. 116, Luminous Stars and Associations in Galaxies, ed. C. W. H. de Loore, A. Willis, & P. Laskarides (Dordrecht: Reidel), 139
Bateson, F. M. 1980–1993, Roy. Astron. Soc. New Zealand, Var. Star Sect. Circ.
Bernat, A. P., & Lambert, D. L. 1978, PASP, 90, 520
Boggess, N. W., et al. 1978, Nature, 275, No. 5679, 372
Capps, R. W., Coyne, G. V., & Dyck, H. M. 1973, ApJ, 184, 173
Caputo, F., & Viotti, R. 1970, A&A, 7, 266
Cassatella, A., et al. 1979, A&A, 79, 223
Cassatella, A., Ponz, D., Selvelli, P. L., & Vogel, M. 1990, NASA, *IUE* Newsletter, 41, 155
Cassinelli, J. P., Nordsieck, K. H., & Murison, M. A. 1987, ApJ, 317, 290
Clampin, M., Nota, A., Golimowski, D., Leitherer, C., & Durrance, S. T. 1993, ApJ, 410, L35
Clarke, D., & McLean, I. S. 1974, MNRAS, 167, 27
Clayton, G. C., et al. 1992, ApJ, 385, L53
Conti, P. S. 1984, in IAU Symp. 105, Observational Tests of Stellar Evolution Theory, ed. A. Maeder & A. Renzini (Dordrecht: Reidel), 233
Davidson, K. 1987, ApJ, 317, 760
———. 1989, in IAU Colloq. 113, Physics of Luminous Blue Variables, ed. K. Davidson, A. F. J. Moffat, & H. J. G. L. M. Lamers (Dordrecht: Kluwer), 101
Davidson, K., Moffat, A. F. J., & Lamers, H. J. G. L. M., eds. 1989, IAU Colloq. 113, Physics of Luminous Blue Variables (Dordrecht: Kluwer),
de Freitas Pacheco, J. A., Damineli, A., Costa, R. D. D., & Viotti, R. 1992, A&A, 266, 360
de Koter, A. 1993, Ph.D. thesis, Univ. of Utrecht
Drissen, L., St.-Louis, N., Moffat, A. F. J., & Bastien, P. 1987, ApJ, 322, 888
Fox, G. K., & Henrichs, H. F. 1994, MNRAS, in press
Gallagher, J. S. 1989, in IAU Colloquium 113, Physics of Luminous Blue Variables, ed. K. Davidson, A. F. J. Moffat, & H. J. G. L. M. Lamers (Dordrecht: Kluwer), 185
Gnedin, Y. N., Kiselev, N. N., Pogodin, M. A., Rozenbush, A. E., & Rozenbush, V. K. 1992, Soviet Astron. Lett., 18, 182
Grady, C. A., & Garhart, M. P. 1988, NASA *IUE* Newsletter, 35, 79
Groenewegen, M. A. T., Lamers, H. J. G. L. M., & Pauldrach, A. W. A. 1989, A&A, 221, 78
Hamann, W.-R. 1987, in Numerical Radiative Transfer, ed. W. Kalkofen (Cambridge: Univ. Press), 35
Hamann, W.-R., & Schmutz, W. 1987, A&A, 174, 173
Hayes, D. P. 1985, ApJ, 289, 726
Hester, J. J., Light, R. M., Westphal, J. A., Currie, D. G., Groth, E. J., Holtzman, J. A., Lauer, T. R., & O'Neil, E. J. Jr., AJ, 102, 654
Hillier, D. J. 1992, in The Atmospheres of Early-Type Stars, ed. U. Heber & C. S. Jeffery (Berlin: Springer), 105
Hillier, D. J., & Allen, D. A. 1992, A&A, 262, 153
Hubeny, I., Štefl, S., & Harmanec, P. 1985, Bull. Astron. Inst. Czechoslovakia, 36, 214
Humphreys, R. M. 1989, in IAU Colloq. 113, Physics of Luminous Blue Variables, ed. K. Davidson, A. F. J. Moffat, & H. J. G. L. M. Lamers (Dordrecht: Kluwer), 3
Humphreys, R. M., Lamers, H. J. G. L. M., Hoekzema, N., & Cassatella, A. 1989, A&A, 218, L17
Hutsemékers, D., & Van Drom, E. 1991a, A&A, 248, 141
———. 1991b, A&A, 251, 620
Israelian, G., & de Groot, M. 1992, in Nonisotropic and Variable Outflows from Stars, ed. L. Drissen, C. Leitherer, & A. Nota (Provo: Brigham Young Univ.), 356
Johansson, S. 1977, MNRAS, 178, 17P
Johnson, H. M. 1976, ApJ, 206, 469
———. 1982, APJS, 50, 551
Johnson, R. H., Barlow, M. J., Drew, J. E., & Brinks, E. 1992, MNRAS, 255, 261
Kilmartin, P. M., & Bateson, F. M. 1991, IAU Circ., No. 5307
Kinney, A. L. 1992, Faint Object Spectrograph Instrument Handbook (Baltimore: STScI)
Klare, G., Neckel, Th., & Schnur, G. 1972, A&AS, 5, 239
Kudritzki, R.-P., Hummer, D. G., Pauldrach, A. W. A., Puls, J., Najarro, F., & Imhoff, J. 1992, A&A, 257, 655
Kurucz, R. L. 1979, ApJS, 40, 1
Lamers, H. J. G. L. M. 1987, in Instabilities in Luminous Early-Type Stars, ed. H. J. G. L. M. Lamers & C. W. H. de Loore (Dordrecht: Reidel), 99
———. 1989, in IA Colloq. 113, Physics of Luminous Blue Variables, ed. K. Davidson, A. F. J. Moffat, & H. J. G. L. M. Lamers (Dordrecht: Kluwer), 135
Lamers, H. J. G. L. M., Hoekzema, N., Trams, N. R., Cassatella, A., & Barylak, M. 1989, in IAU Colloq. 113, Physics of Luminous Blue Variables, ed. K. Davidson, A. F. J. Moffat, & H. J. G. L. M. Lamers (Dordrecht: Kluwer), 271
Lamers, H. J. G. L. M., Korevaar, P., & Cassatella, A. 1985, A&A, 149, 29
Lamers, H. J. G. L. M., & Pauldrach, A. W. A. 1991, A&A, 244, L5
Leitherer, C., Abbott, D. C., & Schmutz, W. 1989, in IAU Coll. 113, Physics of Luminous Blue Variables, ed. K. Davidson, A. F. J. Moffat, & H. J. G. L. M. Lamers (Dordrecht: Kluwer), 109
Leitherer, C., Appenzeller, I., Klare, G., Lamers, H. J. G. L. M., Stahl, O., & Waters, L. B. F. M. 1985, A&A, 153, 168
Leitherer, C., Damineli, A., & Schmutz, W. 1992, in Nonisotropic and Variable Outflows from Stars, ed. L. Drissen, C. Leitherer, & A. Nota (Provo: Brigham Young Univ.), 366

© American Astronomical Society • Provided by the NASA Astrophysics Data System

1994ApJ...428..292L

Leitherer, C., & Langer, N. 1991, in IAU Symp. 148, The Magellanic Clouds, ed. R. Haynes & D. Milne (Dordrecht: Reidel), 480
Leitherer, C., Schmutz, W., Abbott, D. C., Hamann, W.-R., & Wessolowski, U. 1989b, ApJ, 346, 919
Leitherer, C., & Zickgraf, F. J. 1987, A&A, 174, 103
Lupie, O. L. 1994, in preparation
Lupie, O. L., & Nordsieck, K. H. 1987, AJ, 92, 214
Lupie, O. L., & Stockman, H. S. 1988, in Polarized Radiation of Circumstellar Origin, ed. G. V. Coyne, A. M. Magalhães, A. F. J. Moffat, R. E. Schulte-Ladbeck, S. Tapia, & D. T. Wickramasinghe (Vatican City: Vatican Obs.), 705
Maeder, A. 1989, in IAU Colloq. 113, Physics of Luminous Blue Variables, ed. K. Davidson, A. F. J. Moffat, & H. J. G. L. M. Lamers (Dordrecht: Kluwer), 15
Mayall, M. W. 1969, JRASC, 63, 221
McCall, M., L. 1984, MNRAS, 210, 829
McLean, I. S. 1979, MNRAS, 186, 265
McLean, I. S., Coyne, G. V., Frecher, J. E., & Serkowski, K. 1979, ApJ, 231, L141
Meaburn, J., Gehring, G., Walsh, J. R., Palmer, J. W., Lopez, J. A., Bryce, M., & Raga, A. C. 1993, A&A, 276, L21
Mitra, M. P., & Dufour, R. J. 1990, MNRAS, 242, 98
Nota, A., Drissen, L., Clampin, M., Leitherer, C., Pasquali, A., Robert, C., Paresce, F., & Robberto, M. 1994, in Proc. 34th Herstmonceaux Conf., Circumstellar Media in Late Stages of Stellar Evolution, ed. R. E. S. Clegg (Cambridge: Univ. Press), in press
Nota, A., Leitherer, C., Clampin, M., Greenfield, P., Paresce, F., & Golimowski, D. 1992, ApJ, 398, 469
Paresce, F., & Nota, A. 1989, ApJ, 341, L83
Pauldrach, A. W., & Puls, J. 1990, A&A, 237, 409
Poeckert, R., Bastien, P., & Landstreet, J. D. 1979, AJ, 84, 812
Raga, A. C., & Cantó, J. 1989, ApJ, 344, 404
Robert, C., Moffat, A. F. J., Bastien, P., Drissen, L., & St.-Louis, N. 1989, ApJ, 347, 1034
Schaller, G., Schaerer, D., Meynet, G., & Maeder, A. 1992, A&AS, 96, 269
Schmidt, G. D., Elston, R., & Lupie, O. L. 1992, AJ, 104, 1563
Schmutz, W., Hamann, W.-R., & Wessolowski, U. 1989, A&A, 210, 236
Schmutz, W., Leitherer, C., Hubeny, I., Vogel, M., Hamann, W.-R., & Wessolowski, U. 1991, ApJ, 372, 664
Schulte-Ladbeck, R. E., Clayton, G. C., & Meade, M. R. 1993, in Massive Stars: Their Lives in the Interstellar Medium, ed. J. P. Cassinelli & E. B. Churchwell (Provo: Brigham Young Univ.), 237
Schulte-Ladbeck, R. E., Leitherer, C., Clayton, G. C., Robert, C., Meade, M. R., Drissen, L., Nota, A., & Schmutz, W. 1993, ApJ, 407, 723
Schulte-Ladbeck, R. E., Meade, M. R., & Hillier, D. J. 1992, in Nonisotropic and Variable Outflows from Stars, ed. L. Drissen, C. Leitherer, & A. Nova (Provo: Brigham Young Univ.), 118
Serkowski, K. 1968, ApJ, 154, 115
———. 1970, ApJ, 160, 1083
Serkowski, K., Mathewson, D. S., & Ford, V. L. 1975, ApJ, 196, 261 (SMF)
Shore, S. N. 1992, in Nonisotropic and Variable Outflows from Stars, ed. L. Drissen, C. Leitherer, & A. Nota (Provo: Brigham Young Univ.), 342
Shore, S. N., Waxin, Y., & Altner, B. 1994, in preparation
Smith, L. J., Crowther, P. A., & Prinja, R. K. 1994, A&A, in press
Snow, T. P., & Stalio, R. 1987, in Exploring the Universe with the *IUE* Satellite, ed. Y. Kondo (Dordrecht: Reidel), 183
Stahl, O. 1986, A&A, 164, 321
Stahl, O., Mandel, H., Wolf, B., Gäng, Th., Kaufer, A., Kneer, R. Szeifert, Th., & Zhao, F. 1993, A&AS, 99, 167
Stahl, O., Wolf, B., Klare, G., Cassatella, A., Krautter, J., Persi, P., & Ferrari-Toniolo, M. 1983, A&A, 127, 49
Stahl, O., Wolf, B., Klare, G., Jüttner, A., & Cassatella, A. 1990, A&A, 228, 379
Stellingwerf, R. F. 1978, ApJ, 224, 953
Sterken, C., Gosset, E., Jüttner, A., Stahl, O., Wolf, B., & Axer, M. 1991, A&A, 247, 383
Taylor, M., & Cassinelli, J. P. 1992, ApJ, 401, 311
Taylor, M., Nordsieck, K.-H., Schulte-Ladbeck, R. E., & Bjorkman, K. S. 1991, AJ, 102, 1197
Thackeray, A. D. 1950, MNRAS, 110, 526
———. 1969, M.N.A.S. So. Africa, 28, 37
———. 1977, MNRAS, 180, 85
van Genderen, A. M., et al. 1988, A&AS, 74, 453
Viotti, R. 1976, ApJ, 204, 293
Viotti, R., Altamore, A., Barylak, M., Cassatella, A., Gilmozzi, R., & Rossi, C. 1984, in Future of Ultraviolet Astronomy Based on Six Years of *IUE* Research (NASA CP-2349), 231
Warren-Smith, R. F., Scarrott, S. M., Murdin, P., & Bingham, R. G. 1979, MNRAS, 187, 761
White, R. L., & Becker, R. H. 1982, ApJ, 262, 657
Whitelock, P. A., Carter, P. S., Roberts, G., Whittet, D. C. B., & Baines, D. W. T. 1983, MNRAS, 205, 577
Wilking, B. A., Lebofsky, M. J., & Rieke, G. 1982, AJ, 87, 695
Wolf, B. 1989, in IAU Colloq. 113, Physics of Luminous Blue Variables, ed. K. Davidson, A. F. J. Moffat, & H. J. G. L. M. Lamers (Dordrecht: Kluwer), 91
———. 1992, in Nonisotropic and Variable Outflows from Stars, ed. L. Drissen, C. Leitherer, & A. Nota (Provo: Brigham Young Univ.), 327
Wolf, B., Appenzeller, I., & Stahl, O. 1981, A&A, 103, 94
Wolf, B., & Stahl, O. 1982, A&A, 112, 111
Zickgraf, F.-J. 1992, in Nonisotropic and Variable Outflows from Stars, ed. L. Drissen, C. Leitherer, & A. Nota (Provo: Brigham Young Univ.), 75
Zickgraf, F.-J., & Schulte-Ladbeck, R. E. 1989, A&A, 214, 274
Zickgraf, F.-J., Wolf, B., Stahl, O., Leitherer, C., & Klare, G. 1985, A&A, 143, 421

© American Astronomical Society • Provided by the NASA Astrophysics Data System